Extended-soft-core baryon-baryon model ESC16. I. Nucleon-nucleon scattering

M. M. Nagels and Th. A. Rijken
Institute of Mathematics, Astrophysics, and Particle Physics, Radboud University, Nijmegen, The Netherlands

Y. Yamamoto
Nishina Center for Accelerator-Based Science, Insitute for Physical and Chemical Research (RIKEN), Wako, Saitama, 351-0198, Japan

(Received 29 September 2016; revised manuscript received 2 October 2018; published 26 April 2019)

Background: The Nijmegen extended-soft-core (ESC) model ESC16, as well as its predecessors ESC04–ESC08, describe the nucleon-nucleon (NN), hyperon-nucleon (YN), and hyperon-hyperon/nucleon ($YY/\Xi N$) interactions in a unified way using broken SU(3) symmetry. SU(3) symmetry serves to connect the NN with the YN and the YY channels. In the spirit of the Yukawa approach to the nuclear force problem, the interactions are studied from the meson-exchange picture viewpoint, using generalized soft-core Yukawa functions. The meson exchanges are supplemented with diffractive contributions due to multiple-gluon exchanges. The extended-soft-core (ESC) meson-exchange interactions consist of local and nonlocal potentials due to (i) one-boson exchanges (OBE), which are the members of nonets of pseudoscalar, vector, scalar, and axial-vector mesons, (ii) diffractive exchanges, (iii) two-pseudoscalar exchange (PS-PS), and (iv) meson-pair exchange (MPE). The OBE and MPE vertices are regulated by Gaussian form factors producing potentials with a soft behavior near the origin. The assignment of the cutoff masses for the BBM vertices is dependent on the SU(3) classification of the exchanged mesons for OBE and a similar scheme for MPE.
Purpose: The evolution of the ESC approach to the ESC16 model for the baryon-baryon (BB) interactions of the SU(3) flavor octet of baryons (N, Λ, Σ, and Ξ) is described and presented. In this first of a series of papers, the NN model and results are reported in detail.
Methods: Important nonstandard ingredients in the OBE sector in the ESC models are (i) the axial-vector meson potentials, and (ii) a zero in the scalar- and axial-vector meson form factors. Furthermore, the strange scalar κ meson is treated within the scheme of the Gell-Mann-Okubo mass relations, and like the ρ and ϵ treated as a broad meson. The multiple-gluon exchanges are elaborated further by adding contributions due to odd number of gluon exchanges. A novel contribution is the incorporation of structural effects due to the quark core of the baryons. In establishing the parameters of the model a simultaneous fit to NN and YN channels has been performed. The meson-baryon coupling constants are calculated via SU(3) using the coupling constants of the $NN \oplus YN$ analysis as input. In ESC16 the couplings are kept completely SU(3) symmetric. About 25 physical coupling parameters and 8 cutoff and diffractive masses were searched.
Results: In the fit to NN and YN many parameters are essentially fixed by the NN data. A few, but severely constrained parameters, e.g., $F/(F+D)$ ratios, are left for determination of the YN interactions and the YY experimental indications. The simultaneous fit of the ESC models to the NN- and YN-scattering data with a single set of parameters has achieved excellent results for the NN and YN data, and for the YY data in accordance with the experimental indications for $\Lambda\Lambda$ and ΞN. In the case of ESC16, the version discussed here, the achievements are: (i) For the selected 4313 pp and np scattering data with energies $0 \leqslant T_{\rm lab} \leqslant 350$ MeV, the model reaches a fit having $\chi^2/N_{\rm data} = 1.10$. (ii) The deuteron binding energy and all the NN scattering lengths are fitted very nicely. (iii) The YN data are described very well with $\chi^2/N_{\rm data} = 1.04$, giving at the same time a description of the ΞN cross sections in agreement with the experimental indications.
Conclusions: The ESC approach leads to an excellent description of the NN and YN data, and for the scarce YY data. The added innovations as well as the treatment of mass broken SU(3) make it possible to keep the meson coupling parameters and the $F/(F+D)$ ratios of the model qualitatively in accordance with the predictions of the $^3P_0$-dominated quark-antiquark pair creation (QPC) model. The information about estimates of (i) the Λ- and Σ-nuclear well-depth, and (ii) the $\Lambda\Lambda$ hypernuclei played an important role in the form of using constraints. In particular, the experimental indications for the $\Lambda\Lambda$-attraction and the Σ-nuclear well-depth were directive.

DOI: 10.1103/PhysRevC.99.044002

I. INTRODUCTION

In a new series of papers we present the results obtained with the recent ESC16 version of the extended-soft-core (ESC) model [1] for nucleon-nucleon (NN), hyperon-nucleon (YN), and hyperon-hyperon (YY) interactions with $S = 0, -1, -2$. Moreover, we present predictions for the YY channels with $S = -3, -4$.

The combined study of all baryon-baryon (BB) interactions, exploiting all experimental information hitherto available, both on BB-scattering and (hyper-)nuclear systems, might throw light on the basic mechanisms of these interactions. The program, which in its original form was formulated in Refs. [2,3], pursues the following aims:

(i) To study the assumption of broken SU(3) symmetry. For example, we investigate the properties of the scalar mesons [$\varepsilon = f_0(620)$, $f_0(993)$, $\delta = a_0(962)$, $\kappa(861)$].
(ii) To determine the $F/(F+D)$ ratios [4].
(iii) To study the connection between QCD, the quark model, and low-energy physics.
(iv) To extract, in spite of the scarce experimental YN and YY data, information about scattering lengths, effective ranges, the existence of resonances, and bound states, etc.
(v) To provide realistic baryon-baryon potentials, which can be applied in few-body calculations, nuclear and hyperonic matter studies, and neutron stars.
(vi) To extend the theoretical description to the baryon-baryon channels with strangeness $S = -2$; this in particular for the $\Lambda\Lambda$ and ΞN channels, where some data already exist, and for which experiments will be realized in the near future.
(vii) Finally, to extend the theoretical description to all baryon-baryon channels with strangeness $S = -3, -4$. These will be parameter-free predictions, and have, like the other BB-channels, relevance for the study of hyperonic matter and compact stars.

With this series of papers this program nears essentially its completion.

As has been amply demonstrated, see Refs. [5–9], the ESC-model interactions give excellent simultaneous descriptions of the NN and YN data. Also it turned out that the ESC approach gives great improvements for the NN description as compared to the one-boson-exchange (OBE) models, e.g., Refs. [3,10], and other existing models in the literature. The ESC16 model presents the culmination in this respect: the NN model has a quality on equal par with the energy-dependent partial-wave analysis (PWA) [11,12].

The ESC04-model papers [5–7] contain the first rather extensive exposition of the ESC approach. As compared to the earlier versions of the ESC model, we introduced in ESC04 models [5–7] several innovations: First, we introduced a zero in the form factor of the mesons with P-wave quark-antiquark contents, which applies to the scalar and axial-vector mesons. Second, we exploited the exchange of the axial-vector mesons with $J^{\rm PC} = 1^{++}$ and $J^{\rm PC} = 1^{+-}$. Third, we employed some $\Lambda\Lambda$, ΞN information.

In the ESC16 model on top of these improvements, we introduce in the ESC approach for the first time: (i) Odderon exchange $J^{\rm PC} = 1^{--}$. Odderon exchange represents the exchange of an odd-number of gluons at short-distance; this to complement pomeron exchange, which stands for the exchange of an even-number of gluons. (ii) Quark-core effects. The quark-core effects represent structural effects caused by the occurrence of Pauli-blocked configurations in two-baryon systems. These structural effects depend on the BB channel and cannot be described by t-channel exchanges.

Furthermore, (iii) the axial-vector ($J^{\rm PC} = 1^{++}$) mesons are treated with the most general vertices, and the $(\boldsymbol{\sigma}_1 \cdot \mathbf{q})(\boldsymbol{\sigma}_2 \cdot \mathbf{q})$ operator is evaluated in a superior manner compared to ESC04. Not included are the potentials from the tensor ($J^{\rm PC} = 2^{++}$) mesons. Attempts including the latter mesons did not lead to substantial potentials from these mesons or qualitative changes in the other contributions to the potentials. The results with the ESC08 model are reported in Refs. [8,9]. With this simultaneous treatment of the NN, YN, and YY channels we have achieved a high-quality description of the baryon-baryon interactions. The results, using a single set of meson and quark-core parameters, include: (a) a description of the NN data with a $\chi^2_{pdp} = 1.10$ and good low-energy parameters for the NN-channels including the binding energy E_B of the deuteron, (b) a very good fit to the YN-scattering data, (c) the fitting parameters with a clear physical significance, like, e.g., the $NN\pi$-, $NN\rho$-couplings, etc., and with realistic values of the $F/(F+D)$ ratios α_P and α_V^m. The fitting has been done under the constraints of the G-matrix results for the ESC16 interactions. These show (i) satisfactory well-depth values for $U_\Lambda < 0$, $U_\Sigma > 0$, and $U_\Xi < 0$, (ii) proper spin-spin ($U_{\sigma\sigma} \geqslant 1$), and small spin-orbit interactions for ΛN. All these features are in agreement with the Hyperball data [13] and the NAGARA event [14].

In this first paper of the series on the ESC16 model, we display and discuss the NN results of the simultaneous fit to the NN and YN data, including some $\Lambda\Lambda$, ΞN, and ΣN information from hypernuclei, using a single set of parameters. In the second paper, henceforth referred to as II [15], we report on the results for strangeness $S = -1$ YN channels, using the same simultaneous fit of the NN and YN data. This simultaneous fitting procedure was first introduced in Ref. [6], and its importance and advantages will be discussed in II. In the third paper, henceforth referred to as III [16], we report on the results and predictions for YY with strangeness $S = -2$. Finally, in the fourth paper (IV), we describe the predictions for YY with strangeness $S = -3, -4$.

We refer the reader to following sections in Ref. [9] for the descriptions of (a) Sec. III: the two-body integral equations in momentum space and the expansion into Pauli-spinor invariants. (b) Appendix A: the B-field formalism for vector- and axial-vector mesons. (c) Appendix B: the exact treatment of the non-local-tensor operator.

The contents of this paper are as follows. In Sec. II a description of the physical background and dynamical contents of the ESC16 model is given. In Sec. III the momentum-space formalism and structure of the ESC potential are briefly described. Section IV contains some brief remarks on the ESC couplings and the QPC model. In Sec. V the simultaneous $NN \oplus YN \oplus YY$ fitting procedure is reviewed. Here, also the results for the coupling constants and $F/(F+D)$ ratios for OBE and MPE are given. In Sec. VI the NN-results for the ESC16-model are displayed. In Sec. VII we discuss the results and draw some conclusions. In Appendix A the ESC potentials in configuration space for nonstrange mesons are given. In Appendix B the treatment of the nonlocal tensor

potential is reviewed. In Appendix C a short description is given of the QPC derivation of the BBM couplings using Fierz transformations.

II. PHYSICAL CONTENT OF THE ESC MODEL

The general physical basis, within the context of QCD, for the Nijmegen soft-core models has been outlined in the introduction of Ref. [5]. The description of baryon interactions at low energies in terms of baryons and mesons can be reached through the following stages: (i) The strongly interacting sector of the standard model (SM) contains three families of quarks: (ud), (cs), (tb). (ii) Integrating out the heavy quarks (c, b, t) leads to a QCD world with effective interactions for the (u, d, s) quarks. (iii) This QCD world is characterized by a phase transition of the vacuum. Thereby the quarks gets dressed and become the so-called constituent quarks. The emerging picture is that of the constituent-quark model (CQM) [17]. The phase transition has transformed the effective QCD world into an complex hadronic-world. (iv) The strong-coupling-lattice QCD (SCQCD) seems to be a proper model to study the low-energy meson-baryon and baryon-baryon physics; see Ref. [18] for applications and references. Here the lattice spacing $a \geqslant 0.11$ fm provides a momentum scale for which the QCD coupling $g \geqslant 1.1$. Emerging is a picture where the meson-baryon coupling constants get large and quark-exchange effects are rather small. The latter is due to the suppression due to the gluonic overlaps involved. For a similar reason it has been argued [19] that the pomeron is exchanged between the individual quarks of the baryons. In this picture the Nijmegen soft-core approach to baryon-baryon interactions has a natural motivation. (v) For the mesons we restrict ourselves to mesons with $M \leqslant 1.5$ GeV$/c^2$, arriving at a so-called *effective field theory* as the arena for our description of the low-energy baryon-baryon scattering.

In view of the success of QCD, pseudoscalar dominance of the divergence of the axial-vector current (PCAC) leading to small light ("current") quark masses [20,21], the spectroscopic success of the CQM, where the quarks have definite color charges, in generating the masses of the pseudoscalar and vector nonets, and the masses and magnetic moments of the baryon octet is rather surprising [22,23]. The transition from "current" to "constituent" quarks comes from dressing the quark fields in the original QCD Lagrangian; see, e.g., Refs. [17,24,25].

In all works of the Nijmegen group on the baryon-baryon models, (broken) SU(3) flavor-symmetry is explored to connect the NN, YN, and YY channels, making possible a simultaneous fitting of all the available BB data using a single set of model parameters. The dynamical basis is the (approximate) permutation symmetry with respect to the constituent (u, d, s)-quarks. This has its roots in the approximate equality of the quark masses, and more importantly that the gluons have no flavor. This enables the calculation of the baryon-baryon-meson coupling constants using as parameters the nucleon-nucleon-meson couplings and the $F/(F+D)$ ratios. This provides a strong correlation between the (rich) nucleon-nucleon and the (scarce) hyperon-nucleon data.

The obtained coupling constants of the BBM vertices are interpreted studying the predictions of the constituent quark model (CQM) in the form of the quark-antiquark pair creation model (QPC). It has been argued that the $^3P_0$ mechanism [26,27] is dominant over the $^3S_1$ mechanism in lattice QCD [28]. It turned out that the fitted coupling constants in ESC04 and ESC16 indeed follow mainly the pattern of couplings set by the $^3P_0$ model. Also, all $\alpha = F/(F+D)$ ratios are required to deviate no more than 0.1 from the QPC-model predictions for the BBM- and the BB-meson-pair vertices. Although it is in principle attractive to study the SU(3) breaking of the BBM couplings using the QPC model, as has been explored in ESC04 [6], in ESC16 the couplings are treated as SU(3)-symmetric. In the Nijmegen soft-core OBE and ESC models the BBM vertices are described by coupling constants and Gaussian form factors. Given the fact that in the CQM the quark wave functions for the baryons are very much like ground state harmonic oscillator functions, a Gaussian behavior of the form factors is most natural. These form factors guarantee a soft behavior of the potentials in configuration space at small distances. The cutoff parameters in the form factors depend only on the type of meson (pseudoscalar, vector, etc.). Within a meson SU(3) multiplet we distinguish between octet and singlet form factors. Since there is singlet-octet mixing for the $I = 0$ mesons, we attribute the singlet and octet cutoff to the dominant singlet or octet particle, respectively. For the considered nonets the singlet and octet cutoff's are the same or close.

In this way we have full predictive power for the $S = -2, -3, -4$ baryon-baryon channels, e.g., $\Lambda\Lambda$, ΞN channels which involve the singlet {1}-irrep that does not occur in the NN and YN channels.

Field theory allows both linear and nonlinear realizations of chiral-symmetry (CS) [29–31]. At low-energy phenomenologically the nonlinear realization is the most economical and natural. Therefore, we have chosen the pv coupling and not the ps coupling for the pseudoscalar mesons. This choice affects some $1/M^2$ terms in the ps-ps-exchange potential, In ESC04 we tested mixtures of the pv and ps coupling, but in ESC16 we use only the pv coupling. In the nonlinear realization chiral-symmetry for the couplings of the scalar-, vector-, axial-vector-, etc., mesons is realized through isospin symmetry SU(2,I) [30,31].

A. Potentials ESC-model

The potentials of the ESC-model are generated by (i) one-boson-exchange (OBE), (ii) uncorrelated two-meson-exchange (TME), (iii) meson-pair-exchange (MPE), (iv) diffractive/multigluon exchange, (v) quark-core effects (QCE).

(i) The OBE part of the dynamical contents of the ESC16 model is determined by the following meson exchanges:
   (a) $J^{PC} = 0^{--}$: The pseudoscalar-meson nonet π, η, η', K with the $\eta - \eta'$ mixing angle $\theta_P = -11.4^0$ [32], close to the Gell-Mann-Okubo (GMO) quadratic mass formula [33].

(b) $J^{PC} = 1^{--}$: The vector-meson nonet ρ, ϕ, $K^\star$, ω, with the ϕ-ω mixing angle $\theta_V = 39.1^0$ [32]. This follows from the quadratic GMO mass formula and is close to ideal mixing.

(c) $J^{PC} = 1^{++}$: The axial-vector-meson nonet a_1, f_1, K_{1A}, f_1', with the f_1-f_1' mixing angle $\theta_A = 50.0^\circ$ [34].

(d) $J^{PC} = 0^{++}$: The scalar-meson nonet $a_0(962) = \delta$, $f_0(993) = S^\star$, $\kappa(861)$, $f_0(620) = \varepsilon$ [35]. The scalar $S^\star$-ε mixing angle $\theta_S = 44.0^\circ$ is fitted and deviates from the ideal mixing angle $\theta_S = 35.26^\circ$. The $\kappa(861)$ mass is determined via GMO.

(e) $J^{PC} = 1^{+-}$: The axial-vector-meson nonet b_1, h_1, K_{1B}, h_1' with the h_1-h_1' ideal mixing angle $\theta_B = 35.26^\circ$. (Furthermore, $K_{1,A}$ and $K_{1,B}$ are completely mixed.)

The soft-core approach of the OBE has been given originally for NN in Ref. [36], and for YN in Ref. [3]. With respect to these OBE-interactions the ESC-models contain the modification of the form factor by introducing a zero for the mesons being P-wave quark-antiquark states in the CQM: the scalar- and axial-vector mesons. Such a zero is natural in the $^3P_0$-quark-pair-creation (QPC) [26,27] model for the coupling of the mesonic quark-antiquark ($Q\bar{Q}$) system to baryons. A consequence of such a zero is that a bound state in Λp scattering is less likely to occur.

(ii) The configuration space soft-core uncorrelated two-meson exchange for NN has been derived in Refs. [37,38]. Similar to ESC04, also in ESC16 we use these potentials for ps-ps exchange with a complete SU(3)-symmetric treatment in NN, YN, and YY. For example, we include double K exchange in NN scattering. Since this includes two-pion exchange (TPE) the long-range part of the potentials are represented. Here it is tacitly assumed that other TME potentials, like ps-vc, ps-sc, etc., are either small due to cancellations, or can be described adequately by using effective couplings in the OBE potentials. When these effective couplings do not deviate from experimentally determined couplings it may be assumed that the corrections from these other SU(3) meson-nonets in the TME potentials are small. This is our working hypothesis for the TME-potentials. From the point of view of SU(3), since OBE contains only {8}- and {1}-exchange, TME cannot be represented completely in terms of OBE. This because TME also has {27}−, {10}-, and {10*}-exchange components. Therefore, the predictions made by the ESC models could be sensitive to this incompleteness of TME in the ESC models. At present the BB data and the hypernuclear data do not give information at this point.

(iii) Meson-pair exchanges (MPE) have been introduced in Ref. [1] for NN and described in detail in Ref. [39]. The two-meson-baryon-baryon vertices are the low-energy approximations of (a) the heavy-meson and their two-meson decays, and (b) baryon-resonance contributions Δ_{33}, etc. [34,39].

(iv) Diffractive contributions to the soft-core potential have been introduced from the beginning, cf. Ref. [36]. The pomeron is thought of being related to an even number of gluon-exchanges. Here we introduce the odderon potential, which is related to an odd number of gluon exchanges.

(a) $J^{PC} = 0^{++}$: The "diffractive" contribution from the pomeron (P), which is a unitary singlet. These interactions give a repulsive contribution to the potentials in all channels of a Gaussian type.

(b) $J^{PC} = 1^{--}$: The "diffractive" contribution from the odderon (O). The origin of the odderon is assumed to be purely the exchange of the color-singlets with an odd number of gluons. Similar to the pomeron, the odderon potential is taken to be an SU(3) singlet and of the Gaussian form.

As an explanation of the repulsive character of the pomeron-potential the following: The J^{PC} is identical to that for the scalar mesons. Naively, one would expect an attractive central potential. However, considering the two-gluon model for the pomeron [40,41] the two-gluon parallel and crossed diagram contributions to the BB interaction can be shown to cancel adiabatically. The remaining nonadiabatic contribution is repulsive [42].

(v) Quark-core effects in the soft-core model can supply extra repulsion, which may be required in some BB channels. Baryon-baryon studies with the soft-core OBE and ESC models thus far show that it is difficult to achieve a strongly enough repulsive short-range interactions in (i) the $\Sigma^+ p(I = 3/2, {}^3S_1)$ and (ii) the $\Sigma N(I = 1/2, {}^1S_0)$ channel. The short-range repulsion in baryon-baryon may in principle come from: (a) meson- and multi-gluon exchange [5,6], and/or (b) the occurrence of forbidden six-quark SU(6) states by the Pauli principle [43–45]. In view of the mentioned difficulties, we have developed a phenomenological method for the ESC model, which enables us to incorporate this quark-structural effect. This is an important new ingredient of the here presented ESC16 model. This structural effect we describe phenomenologically by Gaussian repulsions, similar to the pomeron. In the ESC16 model we take the strength of this repulsion proportional to the weights of the SU(6) forbidden [51] configuration in the various BB channels. This in contrast to ESC08a,b [8,9], where the quark-core effect is only included in the BB channels with a dominant occurrence of the [51] configuration.

B. Nonlocal potentials, SU(3) breaking, and coulomb

As is well known, the nonlocal potentials are inherent to a relativistic theory, and occur in the central, spin-spin, tensor,

spin-orbit, etc. potentials. In the ESC-models we include the nonlocal contributions to the central/spin-spin potentials for scalar, vector, axial, and diffractive exchanges, as in the OBE models [3,36]. In addition, for all BB-channels we include for the pseudoscalar type of potentials, which occur from pseudoscalar, axial A and B mesons, the nonlocal spin-spin, and tensor contributions [46]. This, because it turned out that the nonlocal pion-exchange spin-spin and tensor force is rather important for achieving a very good fit to the NN data.

The different sources of SU(3) breaking are discussed in paper II of this series.

As in all Nijmegen models, the Coulomb interaction is included exactly, for which we solve the multichannel Schrödinger equation on the physical particle basis. The nuclear potentials are calculated on the isospin basis. This means that we include only the so-called "medium strong" SU(3) breaking and the charge-symmetry breaking (CSB) in the potentials.

III. ESC-MODEL FORMALISM AND POTENTIALS

The two-body momentum-space integral integral equations for baryon-baryon have been given in Refs. [5,9]. Here also the expansion of the scattering amplitude and the potential in Pauli-invariants $V(\mathbf{p}', \mathbf{p}) = \sum_{i=1,8} V_i(\mathbf{p}', \mathbf{p})\, P_i(\mathbf{p}', \mathbf{p})$ is given in detail. The potentials are written in the form

$$V_i(\mathbf{k}^2, \mathbf{q}^2) = \sum_X \Omega_i^{(X)}(\mathbf{k}^2)\Delta^{(X)}(\mathbf{k}^2, m^2, \Lambda^2), \tag{1}$$

where the momentum transfers $\mathbf{k} = \mathbf{p}' - \mathbf{p}$ and $\mathbf{q} = (\mathbf{p}' + \mathbf{p})/2$ with the initial and final state center-of-mass (CM) momenta $\mathbf{p}$, respectively, $\mathbf{p}'$. For the $\Omega_i^{(X)}$ $(i = 1, 8)$ we refer again to Refs. [5,9]. Here X denotes the meson type [pseudoscalar (P), vector (V), scalar (S), axial-vector (A, B)]. Characteristic for the soft-core models is the Gaussian form factor, leading for $X = P,\ V,\ B$, being $q\bar{q}$ s-states, to the "generalized" Yukawa meson-propagator,

$$\Delta^{(X)}(\mathbf{k}^2, m^2, \Lambda^2) = e^{-\mathbf{k}^2/\Lambda^2}/(\mathbf{k}^2 + m^2). \tag{2}$$

Here, m denotes the meson mass, and Λ is the cutoff. (The Gaussian cutoff is responsible for the "softness" of the potentials at short distance.) For $X = S,\ A$, being $q\bar{q}$ p-states, there is a zero in the form factor,

$$\Delta^{(S)}(\mathbf{k}^2, m^2, \Lambda^2) = (1 - \mathbf{k}^2/U^2)e^{-\mathbf{k}^2/\Lambda^2}/(\mathbf{k}^2 + m^2), \tag{3}$$

and for the pomeron and odderon $X = D,\ O$, being multigluon effects,

$$\Delta^{(D)}(\mathbf{k}^2, m^2, \Lambda^2) = \frac{1}{\mathcal{M}^2} e^{-\mathbf{k}^2/(4m_{P,O}^2)}. \tag{4}$$

Here, $\mathcal{M}$ is a scaling mass and set to the proton mass.

In Refs. [5,9] the interaction Hamiltonians for the meson-baryon-baryon couplings are defined. For OBE the detailed expressions of the $\Omega_i^{(X)}$ $(i = 1,\ 6)$ can be found in Refs. [5,9]. The terms with P_7 and P_8 have been neglected.

The complete formulas for the potentials in configuration space are given in Appendix A. These are to be distinguished from those in given in Refs. [5,9] because of a slightly different treatment of the local and nonlocal potentials, using in this work the separation,

$$V_i(\mathbf{k}^2, \mathbf{q}^2) = V_{ia}(\mathbf{k}^2) + V_{ib}(\mathbf{k}^2)(\mathbf{q}^2 + \mathbf{k}^2/4). \tag{5}$$

A. TME and MPE potentials

For TME only the pseudoscalar-pseudoscalar (TPS) potentials are included like in Refs. [5,9]. In the case of the meson-pair-exchange (MPE) potentials included are ps-ps, ps-vc, ps-sc potentials. Because of SU(3) symmetry also for nucleon-nucleon there are contributions from KK-, KK^*-, Kκ-pairs. For a more proper appreciation of the short-range physics of the meson-pair vertices, it is useful to scale the phenomenological meson-pair baryon-baryon interaction Hamiltonians differently from the originally used scalings [38,39]. The Hamiltonians with this new scaling are

$$\begin{aligned}
\mathcal{H}_S &= \bar{\psi}\psi[g_{(\pi\pi)_0}\boldsymbol{\pi}\boldsymbol{\pi} + g_{(\sigma\sigma)}\sigma^2]/\mathcal{M},\\
\mathcal{H}_V &= g_{(\pi\pi)_1}[\bar{\psi}\gamma_\mu\boldsymbol{\tau}\psi](\boldsymbol{\pi} \times \partial^\mu\boldsymbol{\pi}/m_\pi)/\mathcal{M}\\
&\quad -\frac{f_{(\pi\pi)_1}}{2M}[\bar{\psi}\sigma_{\mu\nu}\boldsymbol{\tau}\psi]\partial^\nu(\boldsymbol{\pi} \times \partial^\mu\boldsymbol{\pi}/m_\pi)/\mathcal{M},\\
\mathcal{H}_A &= g_{(\pi\rho)_1}[\bar{\psi}\gamma_5\gamma_\mu\boldsymbol{\tau}\psi]\boldsymbol{\pi} \times \boldsymbol{\rho}/\mathcal{M},\\
\mathcal{H}_P &= g_{(\pi\sigma)}[\bar{\psi}\gamma_5\gamma_\mu\boldsymbol{\tau}\psi](\boldsymbol{\pi}\partial^\mu\sigma - \sigma\,\partial^\mu\boldsymbol{\pi})/(m_\pi\mathcal{M}),\\
\mathcal{H}_B &= ig_{(\pi\omega)}[\bar{\psi}\gamma_5\sigma_{\mu\nu}\boldsymbol{\tau}\psi]\partial^\nu\left(\boldsymbol{\pi}\phi_\omega^\mu\right)/(m_\pi\mathcal{M}).
\end{aligned} \tag{6}$$

Notice that we systematically scaled the partial derivatives with m_π.

B. The Schrödinger equation with nonlocal potential

The nonlocal potentials are an essential part of the baryon-baryon potentials. Without these potentials it is not possible to obtain a very satisfactory fit to the nucleon-nucleon data. In Refs. [36,46] the procedure for the solution in the presence of central, spin-spin, and tensor nonlocal potentials is described. Since the nonlocal tensor potential affects the one-pion-exchange potential (OPEP) it is quite important. Since Ref. [46] is rather unknown, we repeat the treatment in Appendix B.

IV. ESC COUPLINGS AND THE QPC MODEL

It is observed in Ref. [5] that the ESC-coupling constants can be understood in the constituent quark model using the quark-antiquark pair creation process. The $^3P_0$ quark-antiquark pair-creation (QPC) model [26,27] leads to the meson-baryon-baryon couplings rather similar to those found in the fits of the ESC model [5,6]. With an admixture of $^3S_1$ pair creation, the couplings found in the ESC16 model fit very well in the $(^3P_0 + {}^3S_1)$ scheme with a ratio $^3P_0/{}^3S_1 = 2 : 1$.

A. QPC-model coupling nonstrange mesons

According to the quark-pair-creation (QPC) model, in the $^3P_0$ version [26,27], the baryon-baryon-meson couplings are given in terms of the quark-pair creation constant γ_M, and the radii of the (constituent) Gaussian quark wave functions,

TABLE I. Pair-creation constant γ as a function of μ.

μ [GeV]	$\alpha_s(\mu)$	$\gamma(\mu)$
∞	0.00	1.535
80.0	0.10	1.685
35.0	0.20	1.889
1.05	0.30	2.191
0.55	0.40	2.710
0.40	0.50	3.94
0.35	0.55	5.96

by [27,47]

$$g_{\rm BBM}(\pm) = \gamma_{q\bar{q}}\,\frac{3}{\sqrt{2}}\,\pi^{-3/4}\,X_M(I_M,L_M,S_M,J_M)\,F_M^{(\pm)}, \quad (7)$$

where $\pm = -(-)^{L_f}$ with L_f is the orbital angular momentum of the final BM-state, $X_M(\ldots)$ is a isospin, spin, etc., recoupling coefficient, and

$$F^{(+)} = \tfrac{3}{2}\,(m_M R_M)^{+1/2}(\Lambda_{\rm QPC}R_M)^{-2},$$
$$F^{(-)} = \tfrac{3}{2}\,(m_M R_M)^{-1/2}(\Lambda_{\rm QPC}R_M)^{-2}3\sqrt{2}(M_M/M_B), \quad (8)$$

are coming from the overlap integrals; see Appendix C. Here, the superscripts $\mp$ refer to the parity of the mesons M: $(-)$ for $J^{\rm PC} = 0^{+-}$, 1^{--} and $(+)$ for $J^{\rm PC} = 0^{++}$, 1^{++}. The radii of the baryons, in this case nucleons, and the mesons are, respectively, denoted by R_B and R_M.

The QPC($^3P_0$) model gives several interesting relations, such as $g_\omega = 3g_\rho$, $g_\epsilon = 3g_{a_0}$ and $g_{a_0} \approx g_\rho$, $g_\epsilon \approx g_\omega$. These relations can be seen most easily by applying the Fierz-transformation to the $^3P_0$-pair-creation Hamiltonian; see Appendix C.

From $\rho \to e^+e^-$, employing the current-field-identities (CFIs) one can derive, see for example Ref. [48], the following relation with the QPC model:

$$f_\rho = \frac{m_\rho^{3/2}}{\sqrt{2}|\psi_\rho(0)|} \Leftrightarrow \gamma\left(\frac{2}{3\pi}\right)^{1/2}\frac{m_\rho^{3/2}}{|'\psi_\rho(0)'|}, \quad (9)$$

which, neglecting the difference between the wave functions on the left- and right-hand side, gives for the pair creation constant $\gamma \to \gamma_0 = \frac{1}{2}\sqrt{3\pi} = 1.535$. However, since in the QPC model Gaussian wave functions are used, the $q\bar{q}$ potential is a harmonic-oscillator one. This does not account for the $1/r$ behavior, due to one-gluon-exchange (OGE), at short distance. This implies an OG correction [49] to the wave function, which gives for γ [50]

$$\gamma = \gamma_0\left(1 - \frac{16}{3}\frac{\alpha(m_M)}{\pi}\right)^{-1/2}. \quad (10)$$

In Table I $\gamma(\mu)$ is shown, Using from Ref. [51] the parametrization

$$\alpha_s(\mu) = 4\pi/\left[\beta_0 \ln\left(\mu^2/\Lambda^2_{\rm QCD}\right)\right], \quad (11)$$

with $\Lambda_{\rm QCD} = 100\,{\rm MeV}$ and $\beta_0 = 11 - \frac{2}{3}n_f$ for $n_f = 3$, and taking the typical scale $m_M \approx 1$ GeV, the above formula gives $\gamma = 2.19$. This value we will use later when comparing the QPC-model predictions and the ESC16-model coupling constants.

Equations (8) are valid for the most simple QPC model. For a realistic description of the coupling constants of the ESC16-model we include two sophistications: (i) inclusion of both the $^3P_0$ and the $^3S_1$ mechanism, (ii) inclusion of SU(6) breaking. For details, see Ref. [52]. For the latter we use the (56) and (70) SU(6)-irrep mixing [47], and a short-distance quark-gluon form factor. In Table II we show the $^3P_0$-$^3S_1$-model results and the values obtained in the ESC16 fit. In this table we fixed $\gamma_M = 2.19$ for the vector-, scalar-, and axial-vector mesons. From Table I one sees that at the scale of $m_M \approx 1$ GeV such a value is reasonable. Here, one has to realize that the QPC predictions are kind of "bare" couplings, which allows vertex corrections from meson exchange. For the pseudoscalar, a different value has to be used, showing indeed some "running" behavior as expected from QCD. In Ref. [50], for the decays $\rho, \epsilon \to 2\pi$, etc., it was found $\gamma = 3.33$, whereas we have $\gamma_\pi = 5.51$. For the mesonic decays of the charmonium states $\gamma = 1.12$. One notices the similarity between the QPC($^3P_0$)-model predictions and the fitted couplings. Of course, these results are sensitive to the r_M values. We found that for all solutions with a very good χ^2_{NN} the r_M values varied by ± 0.2 fm.

The ESC16 couplings and the QPC couplings agree very well. In particular, the SU(6) *breaking is improving the*

TABLE II. SU(6) breaking in coupling constants, using (56)- and (70)-irrep mixing with angle $\varphi = -22^\circ$ for the $^3P_0$ and $^3S_1$ model. Gaussian quark-gluon cutoff $\Lambda_{\rm QQG} = 986.6\,{\rm MeV}$. Ideal mixing for vector and scalar meson nonets. For pseudoscalar and axial nonets the mixing angles are -11.4° and -42.7°, respectively, imposing the OZI rule. Here, $\Lambda_{\rm QPC} = 259.6\,{\rm MeV}$, $\gamma(\alpha_s = 0.30) = 2.19$, etc. The weights are $A = 0.789$ and $B = 0.211$ for the $^3P_0$ and $^3S_1$, respectively. The values in parentheses in the column QPC denote the results for $\varphi = 0^\circ$.

Meson	$r_M[fm]$	γ_M	$^3S_1$	$^3P_0$	QPC	ESC16
$\pi(140)$	0.30	5.51	$g = -1.37$	$g = +5.12$	3.76 (3.99)	3.65
$\eta'(957)$	0.60	2.22	$g = -1.61$	$g = +6.02$	4.41 (5.38)	4.32
$\rho(770)$	0.80	2.37	$g = -0.09$	$g = +0.65$	0.57 (0.68)	0.58
$\omega(783)$	0.70	2.35	$g = -0.48$	$g = +3.60$	3.12 (3.09)	3.11
$a_0(962)$	0.80	2.22	$g = +0.12$	$g = +0.46$	0.59 (0.61)	0.54
$\epsilon(620)$	0.70	2.37	$g = +0.63$	$g = +2.35$	2.98 (2.98)	2.98
$a_1(1270)$	0.60	2.09	$g = -0.09$	$g = -0.67$	-0.76 (-0.77)	-0.82
$f_1(1285)$	0.60	2.09	$g = -0.08$	$g = -0.60$	-0.68 (-0.69)	-0.76

agreement significantly. All this strengthens the claim that the ESC16 couplings are realistic ones.

B. ESC potentials and the constituent quark model

The calculation of Table II uses the constituent quark model (CQM) in the SU(6) version of Ref. [27]. Since this calculation implicity uses the direct coupling of the mesons to the quarks, it defines the QQM vertex. Then, OBE potentials can be derived by folding meson exchange with the quark wave functions of the baryons. prescribed by the Dirac structure, at the baryon level the vertices have in Pauli-spinor space the $1/\mathrm{M}_B$ expansion,

$$\begin{aligned}\bar{u}(p',s')\Gamma u(p,s) = \chi^{\prime\dagger}_{s'}\Big\{&\Gamma_{bb} + \Gamma_{bs}\frac{\boldsymbol{\sigma}\cdot\mathbf{p}}{E+M} - \frac{\boldsymbol{\sigma}\cdot\mathbf{p}'}{E'+M'}\Gamma_{sb}\\ &-\frac{\boldsymbol{\sigma}\cdot\mathbf{p}}{E+M}\Gamma_{ss}\frac{\boldsymbol{\sigma}\cdot\mathbf{p}'}{E'+M'}\Gamma_{sb}\Big\}\chi_s\\ &\equiv \sum_l c^{(l)}_{BB}\,[\chi^{\prime\dagger}_{s'}O_l(\mathbf{p}',\mathbf{p})\,\chi_s]\,(\sqrt{M'M})^{\alpha_l}\\ &\times (l = bb, bs, sb, ss). \qquad (12)\end{aligned}$$

This expansion is general and does not depend on the internal structure of the baryon. A similar expansion can be made on the quark level, but now with quark masses m_Q and coefficients $c^{(l)}_{QQ}$. It appears that in the CQM, i.e., $m_Q = M_B/3$, the QQM-vertices can be chosen such that the ratios $c^{(l)}_{QQ}/c^{(l)}_{BB}$ are constant for each type of meson [53]. Then, by scaling the couplings these coefficients can be made equal. (Ipso facto this defines a meson-exchange quark-quark interaction.) This shows that the use of the QPC model is consistent with the $1/\mathrm{M}$ expansion.

V. ESC16 MODEL: FITTING $NN \oplus YN \oplus YY$ DATA

In the simultaneous χ^2 fit of the NN, YN, and YY data a *single set of parameters* was used, which means the same parameters for all BB channels. The input NN data are the same as in Ref. [5], and we refer the reader to this paper for a description of the employed phase shift analysis [11,12]. Note that in addition to the NN phases, including their correlations, in the ESC16 model also the NN low-energy parameters and the deuteron binding energy are fitted. The YN data are those used in Ref. [6] with the addition of higher energy data, see paper II. Of course, it is to be expected that the accurate and very numerous NN data essentially fix most of the parameters. Only some of the parameters, for example, certain $F/(F+D)$ ratios, are quite influenced by the YN data. In the fitting procedure the following constraints are applied: (i) A strong restriction imposed on YN models is the absence of $S = -1$ bound states. (ii) During the fitting process sometimes constraints are imposed in the form of "pseudodata" for some YN scattering lengths. These constraints are based on experiences with Nijmegen YN models in the past or to impose constraints from the G-matrix results. In some cases it is necessary to add some extra weight of the YN-scattering data with respect to the NN data in the fitting process. (iii) After obtaining a solution for the scattering data the corresponding model is tested by checking the corresponding G-matrix results for the well depths for $U_\Sigma > 0$ and $U_\Xi < 0$, and sufficient s-wave spin splitting in the U_Λ. If not satisfactory we refit the scattering data, etc. This iterative process implements the constraints from the G-matrix well-depths results and plays a vital role in obtaining the final results of the combined fit. (For the G-matrix approach to hyperon-nucleus systems, see, e.g., Ref. [54].) The fitting process is discussed more elaborately in paper II.

The χ^2 is a very shallow function of the quark-core parameter, which influences only the YN and YY channels. Accordingly solutions have been obtained using different assumptions about the quark-core effects, all with a strength of about 25% of the total diffractive contribution. In previous work [9], models ESC08a and ESC08a″, the solutions were obtained by assuming quark-core effects only for the channels where the [51] component is dominant: $\Sigma^+p(^3S_1, I = 3/2)$, $\Sigma N(^1S_0, I = 1/2)$, and $\Xi N(^1S_0, I = 1)$. The solution ESC16 is obtained by application of the quark-core effects according to Eq. (8.4) in Ref. [9], see paper II for a full description of the Pauli-blocking scheme.

Like in the NN fit, described in Ref. [5], also in the simultaneous χ^2 fit of the NN and YN data, it appeared again that the OBE couplings could be constrained successfully by the "naive" predictions of the QPC model [26,27]. Although these predictions, see Sec. IV, are "bare" ones, we tried to keep during the searches many OBE couplings in the neighborhood of the QPC values. Also, it appeared that we could either fix the $F/(F+D)$ ratios to those as suggested by the QPC model or apply the same restraining strategy as for the OBE couplings.

A. Fitted BB parameters

The treatment of the broad mesons ρ and ϵ is similar to that in the OBE models [3,36]. For the ρ meson the same parameters are used as in these references. However, for the $\epsilon = f_0(620)$ we take in this work the mass $m_\epsilon = 620\,\mathrm{MeV}$ and width $\Gamma_\epsilon = 464\,\mathrm{MeV}$. Using the the Bryan-Gersten "dipole" parameters [55] for the two-pole approximation we get: $m_1 = 455.15919\,\mathrm{MeV}$, $m_2 = 1158.56219\,\mathrm{MeV}$ and $\beta_1 = 0.28193$, $\beta_2 = 0.71807$. Other meson masses are given in Table III. The sensitivity for the values of the cutoff masses of the η and η' is very weak. Therefore, we have set the $\{1\}$-cutoff mass for the pseudoscalar nonet equal to that for the $\{8\}$. Likewise, for the two nonets of the axial-vector mesons, see Table III. Furthermore, we experience a rather shallow dependence on the value of α_P in the range 0.33–0.40. Therefore, we put it at the Cabibbo-theory value 0.365.

Summarizing the parameters we have for baryon-baryon (BB): (i) NN meson couplings: $f_{NN\pi}$, $f_{NN\eta'}$, $g_{NN\rho}$, $g_{NN\omega}$, $f_{NN\rho}$, $f_{NN\omega}$, g_{NNa_0}, $g_{NN\epsilon}$, g_{NNa_1}, f_{NNa_1}, $g_{NNf'_1}$, $f_{NNf'_1}$, f_{NNb_1}, $f_{NNh'_1}$, (ii) $F/(F+D)$ ratios: α^m_V, α_A, (iii) NN pair couplings: $g_{NN(\pi\pi)_1}$, $f_{NN(\pi\pi)_1}$, $g_{NN(\pi\rho)_1}$, $g_{NN\pi\omega}$, $g_{NN\pi\eta}$, $g_{NN\pi\epsilon}$, (iv) diffractive couplings and masslike parameters g_{NNP}, g_{NNO}, f_{NNO}, m_P, m_O, (v) cutoff masses: $\Lambda^P_8 = \Lambda^P_1 = \Lambda^B_8 = \Lambda^B_1$, Λ^V_8, Λ^V_1, Λ^S_8, Λ^S_1, and $\Lambda^A_8 = \Lambda^A_1$.

The pair coupling $g_{NN(\pi\pi)_0}$ was kept fixed at zero. Note that in the interaction Hamiltonians of the pair-couplings Eq. (6)

TABLE III. Meson couplings and parameters employed in the ESC16 potentials. Coupling constants are at $\mathbf{k}^2 = 0$. An asterisk denotes that the coupling constant is constrained via SU(3). The masses and Λ's are given in MeV.

Meson	Mass	$g/\sqrt{4\pi}$	$f/\sqrt{4\pi}$	Λ
π	138.04		0.2684	1030.96
η	547.45		0.1368*	″
η'	957.75		0.3181	″
ρ	768.10	0.5793	3.7791	680.79
ϕ	1019.41	−1.2384*	2.8878*	″
ω	781.95	3.1149	−0.5710	734.21
a_1	1270.00	−0.8172	−1.6521	1034.13
f_1	1420.00	0.5147	4.4754	″
f_1'	1285.00	−0.7596	−4.4179	″
b_1	1235.00		−2.2598	1030.96
h_1	1380.00		−0.0830*	″
h_1'	1170.00		−1.2386	″
a_0	962.00	0.5393		830.42
f_0	993.00	−1.5766*		″
ε	620.00	2.9773		1220.28
Pomeron	212.06	2.7191		
Odderon	268.81	4.1637	−3.8859	

the partial derivatives are scaled by m_π, and there is a scaling mass $\mathcal{M} = M_N$.

The ESC model described here is fully consistent with SU(3) symmetry using a straightforward extension of the NN model to YN and YY. This is the case for the OBE and TPS potentials, as well as for the pair potentials. For example, $g_{(\pi\rho)_1} = g_{A_8VP}$, and besides $(\pi\rho)$ pairs one sees also that $KK^*(I = 1)$ and $KK^*(I = 0)$ pairs contribute to the NN potentials. All $F/(F + D)$ ratios are taken as fixed with heavy-meson saturation in mind. The approximation we have made in this paper is to neglect the baryon mass differences in the TPS potentials, i.e., we put $m_\Lambda = m_\Sigma = m_N$. This is because we have not yet worked out the formulas for the inclusion of these mass differences, which is straightforward in principle.

B. Coupling constants, $F/(F + D)$ ratios, and mixing angles

The ESC16 meson masses, cutoff parameters, and (fitted) meson-nucleon-nucleon couplings are shown in Table III. Notice that the axial-vector couplings for the B-mesons are scaled with m_{B_1}. For the pseudoscalar, vector, and scalar mesons the mixing, as well as the handling of the diffractive potentials, has been described elsewhere, see, e.g., Refs. [3,10].

In paper II [15] the SU(3) singlet and octet couplings are listed, and also the $F/(F + D)$ ratios and mixing angles. Also the Pauli-blocking effect parameter $a_{\rm PB}$, described in Ref. [9], Sec. VIII, for ESC16 is given. As mentioned above, we searched for solutions where all OBE couplings are compatible with the QPC predictions. This time the QPC model contains a mixture of the $^3P_0$ and $^3S_1$ mechanism, whereas in Ref. [5] only the $^3P_0$ mechanism was considered. For the pair couplings all $F/(F + D)$ ratios were fixed to the predictions of the QPC model.

TABLE IV. Pair-meson coupling constants employed in the ESC16 MPE potentials. Coupling constants are at $\mathbf{k}^2 = 0$. The F/(F+D) ratio are QPC predictions, except that $\alpha_{(\pi\omega)} = \alpha_P$, which is very close to QPC.

$J^{\rm PC}$	SU(3)-irrep	$(\alpha\beta)$	$g/4\pi$	$F/(F + D)$
0^{++}	$\{1\}$	$g(\pi\pi)_0$	–	–
0^{++}	″	$g(\sigma\sigma)$	–	–
0^{++}	$\{8\}_s$	$g(\pi\eta)$	−0.6894	1.000
1^{--}	$\{8\}_a$	$g(\pi\pi)_1$	0.2519	1.000
		$f(\pi\pi)_1$	−1.7762	0.400
1^{++}	″	$g(\pi\rho)_1$	5.7017	0.400
1^{++}	″	$g(\pi\sigma)$	−0.3899	0.400
1^{++}	″	$g(\pi P)$	–	–
1^{+-}	$\{8\}_s$	$g(\pi\omega)$	−0.3287	0.365

One notices that all the BBM α's have values rather close to that which are expected from the QPC model. In the ESC16 solution, $\alpha_A \approx 0.383$, which is close to $\alpha_A \sim 0.4$. As in previous works, e.g., Ref. [36], $\alpha_V^e = 1$ is kept fixed. Above, we remarked that the axial-nonet parameters may be sensitive to whether or not the heavy pseudoscalar nonet with the $\pi(1300)$ are included.

In Table IV we listed the fitted Pair couplings for the MPE potentials. We recall that only one-pair graphs are included, to avoid double counting; see Ref. [5]. The $F/(F + D)$ ratios are all fixed, assuming heavy-boson domination of the pair vertices. The ratios are taken from the QPC model for $Q\bar{Q}$ systems with the same quantum numbers as the dominating boson. For example, the α parameter for the axial $(\pi\rho)_1$ pair could be fixed at the quark-model prediction 0.40; see Table IV. The BB-pair couplings are calculated, assuming unbroken SU(3) symmetry, from the NN-pair coupling and the $F/(F + D)$ ratio using SU(3). Unlike in Refs. [38,39], we did not fix pair couplings using a theoretical model, e.g., based on heavy-meson saturation and chiral-symmetry. So, in addition to the 14 parameters used in Refs. [38,39] we now have six pair-coupling fit parameters. In Table IV the fitted pair couplings are given. Note that the $(\pi\pi)_0$ coupling gets a nonzero contribution from the $\{8_s\}$-pairs, giving $g_{(\pi\pi)_0} = -0.688/2 \approx -0.34$, which is opposite in sign compared to the result in Refs. [38,39]. The $f_{(\pi\pi)_1}$-pair coupling has the opposite sign as compared to Refs. [38,39]. In a model with a more complex and realistic meson dynamics [34] this coupling is predicted as found in the present ESC fit. The $(\pi\rho)_1$ coupling is large as expected from A_1 saturation; see Refs. [38,39]. We conclude that the pair couplings are in general not well understood quantitatively and deserve more study.

In Table III we show the OBE-coupling constants and the Gaussian cutoffs Λ. The used $\alpha =: F/(F + D)$ ratios for the OBE couplings are: pseudoscalar mesons $\alpha_P = 0.365$, vector mesons $\alpha_V^e = 1.0, \alpha_V^m = 0.4655$, scalar-mesons $\alpha_S = 1.0$, and axial mesons $\alpha_A = 0.3830$ and $\alpha_B = 0.4$. In Table IV we show the MPE-coupling constants. The used $\alpha =: F/(F + D)$ ratios for the MPE couplings are: $(\pi\eta)$ pairs $\alpha(\{8_s\}) = 1.0$, $(\pi\pi)_1$ pairs $\alpha_V^e(\{8\}_a) = 1.0, \alpha_V^m(\{8\}_a) = 0.400$, and the $(\pi\rho)_1$ pairs $\alpha_A(\{8\}_a) = 0.400$. The $(\pi\omega)$ pairs $\alpha(\{8_s\})$ has been set equal to $\alpha_P = 0.365$.

TABLE V. ESC16 nuclear-bar pp and np phases in degrees.

$T_{\rm lab}$	0.38	1	5	10	25	50	100	150	215	320
$^1S_0(np)$	54.57	62.02	63.47	59.72	50.48	39.82	25.45	15.11	4.65	−8.34
$^1S_0$	14.62	32.62	54.75	55.16	48.67	38.97	25.06	14.85	4.44	−8.53
$^3S_1$	159.39	147.77	118.25	102.72	80.81	63.03	43.62	31.27	19.58	5.83
ϵ_1	0.03	0.11	0.68	1.17	1.82	2.15	2.50	2.94	3.64	4.93
$^3P_0$	0.02	0.14	1.61	3.81	8.81	11.80	9.68	4.83	−1.86	−11.73
$^3P_1$	−0.01	−0.08	−0.89	−2.04	−4.89	−8.29	−13.28	−17.35	−21.87	−27.90
$^1P_1$	−0.05	−0.19	−1.50	−3.07	−6.39	−9.81	−14.65	−18.75	−23.38	−29.44
$^3P_2$	0.00	0.02	0.22	0.67	2.51	5.80	10.90	14.04	16.24	17.07
ϵ_2	−0.00	−0.00	−0.05	−0.20	−0.81	−1.71	−2.71	−2.99	−2.84	−2.18
$^3D_1$	−0.00	−0.01	−0.18	−0.68	−2.83	−6.51	−12.40	−16.69	−20.72	−25.04
$^3D_2$	0.00	0.01	0.22	0.85	3.70	8.93	17.22	22.15	24.99	25.05
$^1D_2$	0.00	0.00	0.04	0.17	0.69	1.70	3.78	5.70	7.64	9.20
$^3D_3$	0.00	0.00	0.00	0.00	0.03	0.24	1.17	2.31	3.61	4.86
ϵ_3	0.00	0.00	0.01	0.08	0.55	1.59	3.46	4.81	5.97	6.99
$^3F_2$	0.00	0.00	0.00	0.01	0.11	0.34	0.80	1.10	1.14	0.39
$^3F_3$	−0.00	−0.00	−0.01	−0.03	−0.23	−0.67	−1.46	−2.06	−2.66	−3.50
$^1F_3$	−0.00	−0.00	−0.01	−0.06	−0.41	−1.10	−2.11	−2.77	−3.46	−4.69
$^3F_4$	0.00	0.00	0.00	0.00	0.02	0.12	0.51	1.04	1.80	3.00
ϵ_4	−0.00	−0.00	−0.00	−0.00	−0.05	−0.19	−0.53	−0.83	−1.13	−1.46
$^3G_3$	−0.00	−0.00	−0.00	−0.00	−0.05	−0.26	−0.93	−1.73	−2.77	−4.17
$^3G_4$	0.00	0.00	0.00	0.01	0.17	0.71	2.11	3.52	5.17	7.28
$^1G_4$	0.00	0.00	0.00	0.00	0.04	0.15	0.41	0.69	1.06	1.70
$^3G_5$	−0.00	−0.00	−0.00	−0.00	−0.01	−0.05	−0.16	−0.25	−0.28	−0.19
ϵ_5	0.00	0.00	0.00	0.00	0.04	0.20	0.70	1.22	1.83	2.62

VI. ESC16 MODEL, *NN* RESULTS

A. Nucleon-nucleon fit, low-energy, and phase parameters

The NN-fitting procedure is discussed in detail in Ref. [5]. The model is fitted to the 1993 Nijmegen representation of the χ^2 hypersurface of the NN scattering data below $T_{\rm lab} = 350$ MeV [11,12]. Also, the low-energy parameters are fitted for pp, np, and nn. Furthermore, simultaneously the YN data are fitted, using the same set of parameters. As a result, we obtained for ESC16 for the phase shifts $\chi^2/N{\rm data} = 1.10$. For a comparison with Ref. [5], and for use of this model for the description of NN, we give in Table V the nuclear-bar phases for pp in case $I = 1$, and for np in the case of $^1S_0(I = 1)$ and the $I = 0$ phases.

The deuteron has been included in the fitting procedure, as well as the low-energy parameters. The fitted binding energy $E_B = 2.224636$ MeV, which is very close to E_B(experiment) $= 2.224644$ MeV. The charge-symmetry breaking is described phenomenologically by having next to $g_{\rho nn}$ free couplings for $g_{\rho np}$ and $g_{\rho pp}$. This phenomenological treatment is successful for the various NN channels, especially for the $np(^1S_0, I = 1)$ phases, which were included in the NN fit.

We emphasize that we use the single-energy (s.e.) phases and χ^2 surface [12] as a means to fit the NN data. The multi-energy (m.e.) phases of the PW-analysis [11] in Figs. 1–4 are the dashed lines in these figures. One notices that the central value of the s.e. phases do not correspond to the m.e. phases in general, illustrating that there has been a certain amount of noise fitting in the s.e. PW-analysis, see, e.g., ϵ_1 and $^1P_1$ at $T_{\rm lab} = 100$ MeV. The m.e. PW-analysis reaches $\chi^2/N_{\rm data} = 0.99$, using 39 phenomenological parameters plus normalization parameters. The related phenomenological PW-potentials NijmI,II and Reid93 [57], with, respectively, 41, 47, and 50 parameters, turn out all with χ^2/Ndata $= 1.04$. This should be compared to the ESC-model, which has $\chi^2/N_{\rm data} = 1.10$ using for NN 32 meson related parameters. These are 14 QPC-constrained meson-nucleon-nucleon couplings, 6 meson-pair-nucleon-nucleon couplings, 6 Gaussian cutoff parameters, 3 diffractive couplings, and 2 diffractive mass parameters. The three remaining fitting parameters [2 F/(F+D) ratios and the Pauli blocking fraction] are mainly or totally determined by the YN fit. From the figures it is obvious that the ESC model deviates from the m.e. PW analysis in particular at the highest energy.

In Table VI the results for the low-energy parameters are given. To discriminate between the $^1S_0$ wave for pp, np, and nn, we introduced some charge independence breaking by taking $g_{pp\rho} \neq g_{np\rho} \neq g_{nn\rho}$. With this device we fitted the difference between the $^1S_0(pp)$ and $^1S_0(np)$ phases, and the different scattering lengths and effective ranges as well. We found $g_{np\rho} = 0.5427$, $g_{pp\rho} = 0.5932$, which are not far from $g_{nn\rho} = 0.5793$; see Table III. The NN low-energy parameters are described very well; see Table VI. Here, with the exception of a_{nn} and r_{nn} the experimental values are taken from the compilation given in Ref. [58]. For $a_{nn}(^1S_0)$ we have used in the fitting the value from an investigation of the n-p and n-n final state interaction in the $^2H(n, nnp)$ reaction at 13 MeV [59]. The value for $a_{nn}(^1S_0)$ is still somewhat in discussion. Another recent determination [60] obtained, e.g., $a_{nn}(^1S_0) = -16.27 \pm 0.40$ fm. The ESC16 model has the value -17.78 fm which is in between these values. Although the values from Ref. [58] are not recent, here they still give an adequate presentation since this ESC model is not detailed

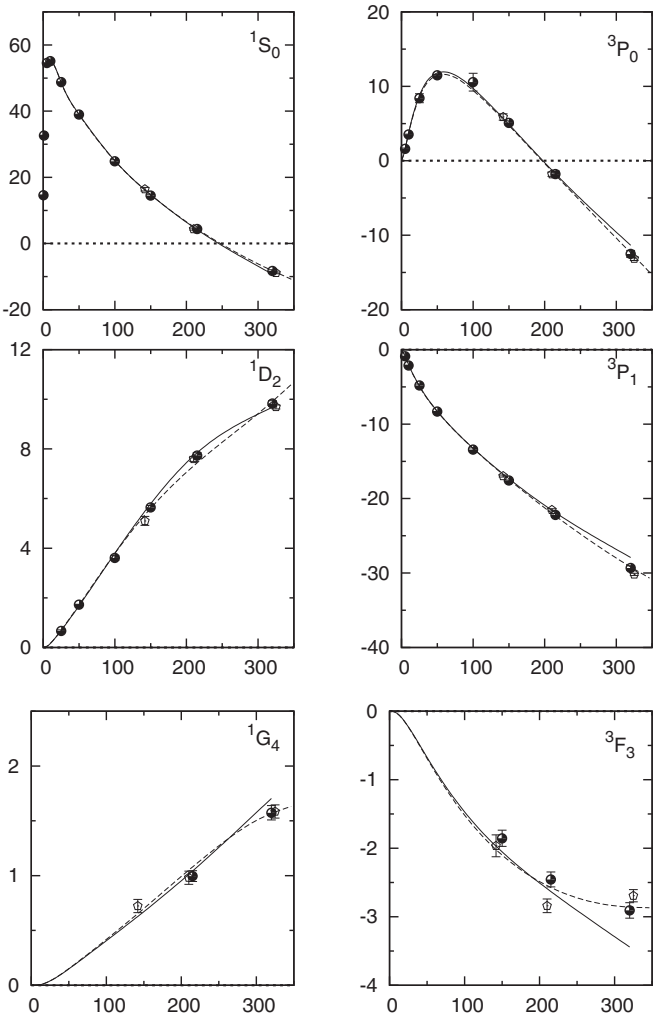

FIG. 1. Solid line: proton-proton $I = 1$ phase shifts in degrees vs. T_{lab} in MeV for the ESC16-model. The dashed line: the multi-energy (m.e.) phases of the Nijmegen93 PW-analysis [11]. The black dots: the single energy (s.e.) phases of the Nijmegen93 PW-analysis. The diamonds: Bugg s.e. [56].

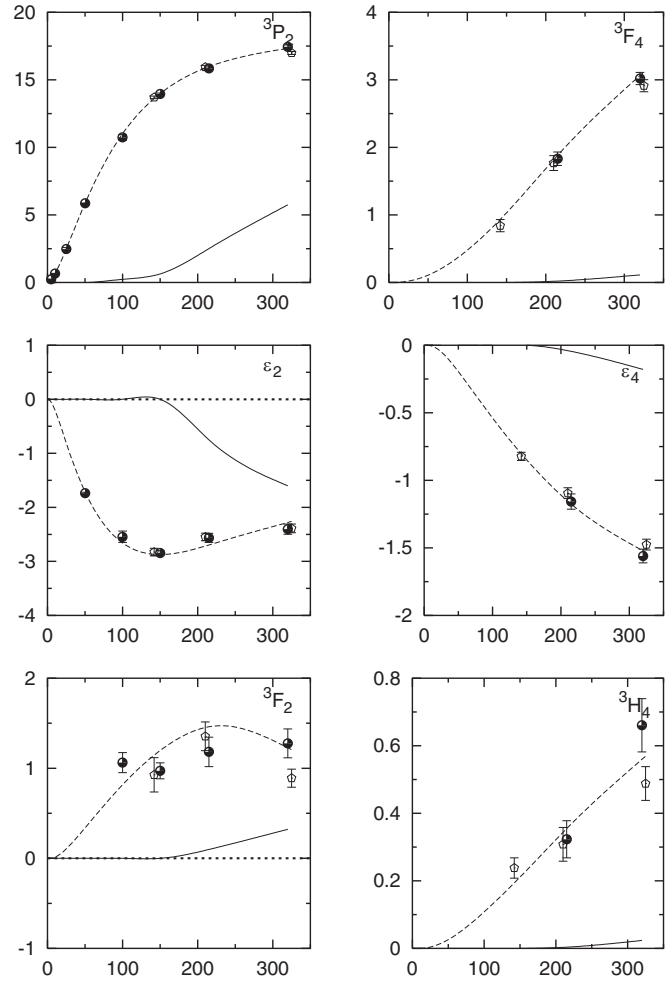

FIG. 2. Solid line: proton-proton $I = 1$ phase shifts in degrees vs. T_{lab} in MeV for the ESC16 model. The dashed line: the m.e. phases of the Nijmegen93 PW analysis [11]. The black dots: the s.e. phases of the Nijmegen93 PW analysis. The diamonds: Bugg s.e. [56].

study of the low-energy parameters. For a discussion of the theoretical and experimental situation with respect to these low-energy parameters, see Ref. [61]. The binding energy of the deuteron is fitted excellently. The electric quadrupole moment result is typical for models without meson-exchange current effects. Further properties of the deuteron in this model are: $P_D = 6.15\%$, $D/S = 0.025698$, $N_G^2 = 0.771658$, and $\rho_{-\epsilon,-\epsilon} = 1.725857$. In Table VII details on the χ^2 contributions are given. Here, $\Delta\chi^2$ denotes the accressence in χ^2 of the ESC-model w.r.t. the phase shift ananlysis [11,12].

B. Nucleon-nucleon potentials[1]

The nucleon-nucleon OBE, TPS, and pair potentials are qualitatively rather similar in character as the hyperon-nucleon potentials, which are shown in Ref. [6] for the ESC04 model. Therefore, we refer the reader to this cited YN paper for pictures of the potentials. The odderon and the derivative axial-vector coupling, and the nonlocal pseudoscalar type i spin-spin and tensor potentials are added.

The odderon potential is a novel feature of ESC16 model. In Fig. 5 the central and spin-orbit potentials are shown. The spin-spin, tensor, and quadratic spin-orbit potentials are very small. One notices from this figure that the pomeron potential is like an "antiscalar" potential, whereas the odderon is a normal vector-exchange potential. Note the strong cancellation in the spin-orbit giving a negligible summed contribution. The upshot is a universal central repulsion from the pomeron+odderon. In ESC models the strength of the pomeron is related to that of the ε. The pomeron curve in Fig. 5 corresponds to a fit with $\varepsilon = f_0(760)$, whereas in this paper we have $\varepsilon = f_0(620)$. This results in weaker couplings of ε, ω, and pomeron, reducing the strength of the pomeron by $\approx 2/3$.

[1]FORTRAN code ESC2016/NNPOTESC16, Open-access website, NN-Online: http://nn-online.org.

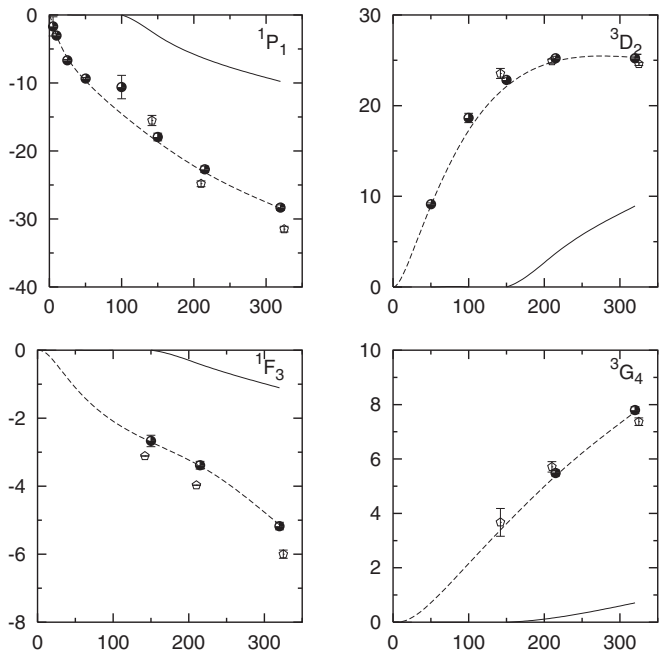

FIG. 3. Solid line: neutron-proton $I = 0$, and the $I = 1$ $^1S_0(NP)$ phase shifts in degrees vs. T_{lab} in MeV for the ESC16 model. The dashed line: the m.e. phases of the Nijmegen93 PW analysis [11]. The black dots: the s.e. phases of the Nijmegen93 PW analysis. The diamonds: Bugg s.e. [56].

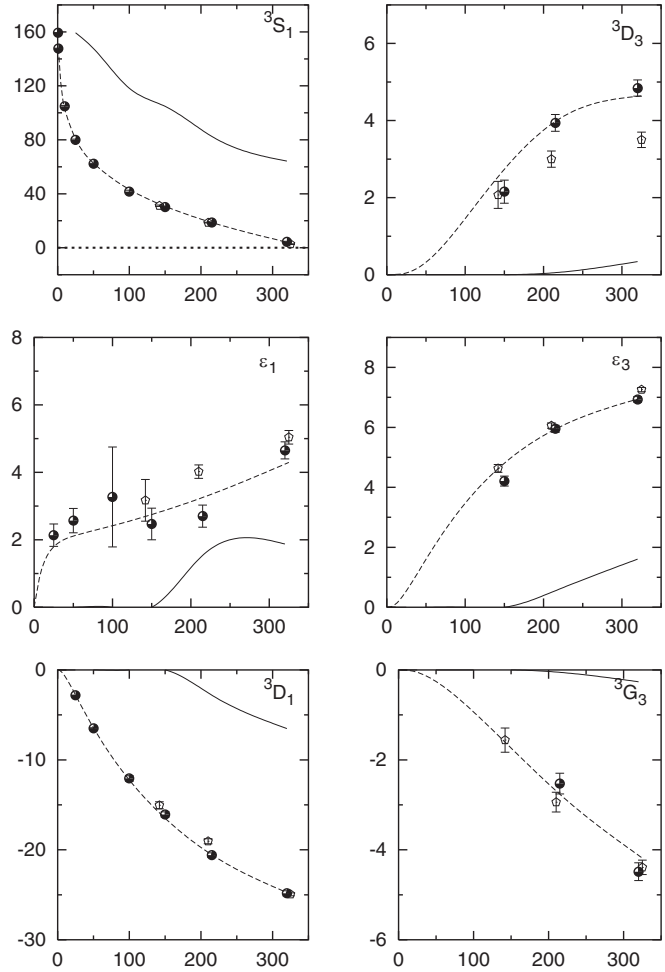

FIG. 4. Solid line: neutron-proton $I = 0$ phase shifts in degrees vs. T_{lab} in MeV for the ESC16 model. The dashed line: the m.e. phases of the Nijmegen93 PW-analysis [11]. The black dots: the s.e. phases of the Nijmegen93 PW-analysis. The diamonds: Bugg s.e. [56].

VII. DISCUSSION AND CONCLUSIONS

The ESC approach to baryon-baryon (BB) interactions is a meson-exchange model with (physical) form factors. Here, besides pseudoscalar also vector, scalar, and axial-vector mesons are included, which is important for an accurate description of the phase shifts at the higher energies. Also, in this approach flavor SU(3) (broken) symmetry can be incorporated to connect the different BB channels. Since [5,9] discussed already the general overall features of the ESC approach, we restrict ourselves to some particular remarks and recent developments.

A presentation of the potentials, valid at low energies, can be obtained by making a low-t expansion of the vector, etc., meson propagators and form factors giving contact terms. This would be similar to the EFT approach [62]. It is to be noted that in the ESC approach a successful description of both the NN- and YN-scattering data is obtained with meson-baryon coupling parameters that can be understood within the QPC model. This is particularly the case for the $F/(F + D)$ ratios of the OBE and MPE interactions, making it unnecessary to introduce extra parameters for the meson-pair vertices. Also, the QPC model treats the scalar mesons on an equal footing with the pseudoscalar, vector, etc., mesons, i.e., as a quark-antiquark bound state. Apart from its role in $\pi\pi$ and πK scattering, the $f_0(620)$ has been shown to be present in relativistic nuclear scattering as well [63]. We note that by studying the relation between the QPC processes and the BBM couplings, we determined the ratio $\gamma(^3P_0)/\gamma(^3S_1) = 2 : 1$. In the literature, the $^3P_0$-QPC and the $^3S_1$-QPC in the

TABLE VI. ESC16 low-energy parameters: S-wave scattering lengths and effective ranges, deuteron binding energy E_B, and electric quadrupole Q_e. Experimental values and references; see Refs. [58,59]. The asterisk denotes that the low-energy parameters were not searched.

	experimental data			ESC16
$a_{pp}(^1S_0)$	−7.828	±	0.008	−7.7718
$r_{pp}(^1S_0)$	2.800	±	0.020	2.7612*
$a_{np}(^1S_0)$	−23.748	±	0.010	−23.7346
$r_{np}(^1S_0)$	2.750	±	0.050	2.6992*
$a_{nn}(^1S_0)$	−18.63	±	0.48	−17.783
$r_{nn}(^1S_0)$	2.860	±	0.15	2.8301*
$a_{np}(^3S_1)$	5.424	±	0.004	5.4396*
$r_{np}(^3S_1)$	1.760	±	0.005	1.7488*
E_B	−2.224644	±	0.000046	−2.224636
Q_e	0.286	±	0.002	0.2727

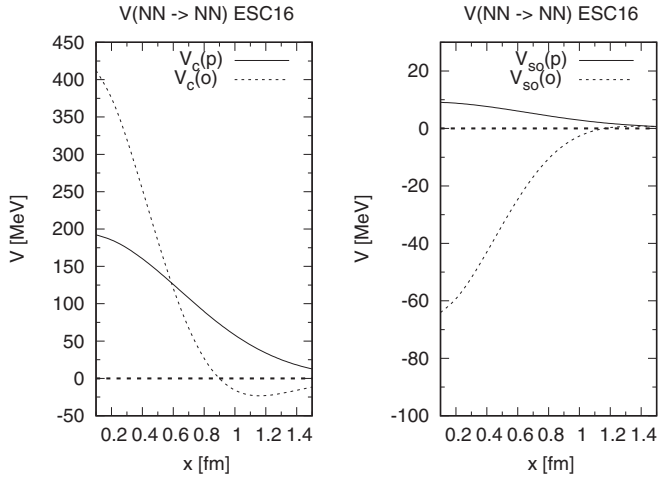

FIG. 5. Pomeron (p) and odderon (o) central- and spin-orbit potentials.

SCQCD [18] has been studied in Refs. [64] and [65], respectively. In this paper we give therefore an estimation of the relative importance of the QPC processes. At the same time we comply with the strong constraint of no bound states in the $S = -1$ systems.

In fitting the NN data the Nijmegen PWA(1993) is used. Although phase shift analyses, with a more extended data base comprising more recent data, e.g., Ref. [66], are available in principle, we expect apart from fine-tuning no major changes. For example, it appeared that measured spin correlations like A_{xx} and A_{yy} from Ref. [67], respectively, Ref. [68], are successfully described by PWA(1993). In Fig. 2 of Ref. [66] the Granada phase shifts are compared to the Nijmegen PWA(1993). From this figure it is clear that both analyses overlap very strongly.

As is well known, the experimental nuclear saturation properties, the density ρ_N, the binding energy per nucleon E/A, and the compression modulus K, cannot be reproduced

TABLE VII. ESC16 χ^2 and χ^2 per datum at the ten energy bins for the Nijmegen93 partial-wave analysis. $N_{\rm data}$ lists the number of data within each energy bin. The bottom line gives the results for the total 0–350 MeV interval. The χ^2 accrescence for the ESC model is denoted by $\Delta\chi^2$ and $\Delta\hat{\chi}^2$, respectively.

$T_{\rm lab}$	$N_{\rm data}$	χ_0^2	$\Delta\chi^2$	$\hat{\chi}_0^2$	$\Delta\hat{\chi}_0^2$
0.383	144	137.555	18.7	0.960	0.130
1	68	38.019	57.3	0.560	0.843
5	103	82.226	7.5	0.800	0.073
10	290	257.995	29.8	1.234	0.103
25	352	272.197	32.6	0.773	0.093
50	571	538.522	33.5	0.957	0.059
100	399	382.499	20.9	0.959	0.052
150	676	673.055	82.6	0.996	0.122
215	756	754.525	132.7	0.998	0.176
320	954	945.379	254.1	0.991	0.266
Total	4313	4081.971	669.8	0.948	0.153

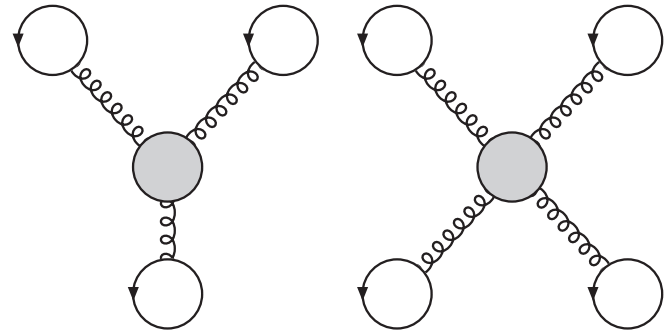

FIG. 6. Triple- and quartic-pomeron three- and four-body interactions.

quantitatively with nuclear two-body interactions only; see, e.g., Ref. [69]. The inclusion of many-nucleon interactions is essential for giving the correct energy curve $E(\rho_N)$. Here, the three-nucleon interaction, composed of an attractive (TNA) and a repulsive (TNR) part, seems to be most important. Soft-core two-baryon potentials lead to a too soft equation of state (EoS). For example, ESC16 gives for the mass of the neutron star $1.35M_\odot$ [70], implying for this model the necessity for a TNR contribution. Furthermore, at high densities hyperon-mixing in neutron-star matter brings about a significant softening of the EoS, which gives a reduction of the TNR effect for the maximum mass [71–73]. To compensate for this adverse effect Nishizaki, Takatsuka, and one of the authors (Y.Y.) [73] made the conjecture that there is a three-baryon repulsion (TBR) that operates universally for YNN and YYN as well as for NNN. In QCD the gluons are flavor blind and therefore it is natural to relate this universal TBR to multigluon exchange. Because in QCD the pomeron is a (nonperturbative) multigluon effect, which gives repulsion at low energies, we associate TBR with triple and quartic pomeron exchange [74,75], as illustrated in Fig. 6.

Then, to stiffen the EoS, together with a phenomenological TNA, we include in the G-matrix matter calculations with ESC16 the universal repulsive multi-gluon three-body (and four-body) forces in the form of the multipomeron exchange potential (MPP) [9,76,77]. As demonstrated in Refs. [78–81], the inclusion of TNA+MPP gives the proper nuclear saturation point and makes the EoS of neutron matter stiff enough to assure the large observed values of two massive neutron stars with mass $1.97 \pm 0.04M_\odot$ for PSR J1614-2230 [82] and $2.01 \pm 0.04M_\odot$ for PSR J0348+0432 [83]. So, with the introduction of TNA+MPP three things are achieved: (i) the right nuclear saturation point, (ii) the proper description of the neutron star masses, and moreover (iii) better hyperonic well depth's U_Y for $Y = \Lambda, \Sigma$ (see the companion paper II).

The combined fit for NN and YN is extremely good in ESC16. It is for the first time that the quality of the NN fit does not suffer from the inclusion of the YN data. The ΛN p-waves seem to be better, which is the result of the truly simultaneous $NN + YN$ fitting. This is also reflected in the better Scheerbaum K_Λ-value [84], making the well-known small spin-orbit splitting smaller; see Ref. [85].

Finally, it is important to stress the role of the information on hypernuclei in our analysis. In the simultaneous fit to the NN and YN data the G-matrix results for hypernuclei constrained the possible solutions. Namely, conditions imposed on the ESC16 solutions are: (i) no BB-bound states, (ii) $U_{ss} > 1$ and $U_\Sigma > 0$.

ACKNOWLEDGMENTS

We thank E. Hiyama, K. Itonaga, T. Motoba, and H.-J. Schulze for many stimulating discussions. Th.A.R. is grateful for the interest and collaboration with R. A. Bryan on the scalar mesons.

APPENDIX A: ONE-BOSON-EXCHANGE INTERACTIONS IN CONFIGURATION SPACE I

In configuration space the BB interactions are described by potentials of the general form[2]

$$V = V_C(r) + V_\sigma(r)\boldsymbol{\sigma}_1\cdot\boldsymbol{\sigma}_2 + V_T(r)S_{12} + V_{SO}(r)\mathbf{L}\cdot\mathbf{S} + V_Q(r)Q_{12} + V_{ASO}(r)\frac{1}{2}(\boldsymbol{\sigma}_1-\boldsymbol{\sigma}_2)\cdot\mathbf{L} - \frac{1}{2M_YM_N}(\boldsymbol{\nabla}^2V^{\text{n.l.}}(r) + V^{\text{n.l.}}(r)\boldsymbol{\nabla}^2), \tag{A1a}$$

$$V^{\text{n.l.}} = \{\varphi_C(r) + \varphi_\sigma(r)\boldsymbol{\sigma}_1\cdot\boldsymbol{\sigma}_2 + \varphi_T(r)S_{12}\}, \tag{A1b}$$

where

$$S_{12} = 3(\boldsymbol{\sigma}_1\cdot\hat{r})(\boldsymbol{\sigma}_2\cdot\hat{r}) - (\boldsymbol{\sigma}_1\cdot\boldsymbol{\sigma}_2), \tag{A2a}$$

$$Q_{12} = \tfrac{1}{2}[(\boldsymbol{\sigma}_1\cdot\mathbf{L})(\boldsymbol{\sigma}_2\cdot\mathbf{L}) + (\boldsymbol{\sigma}_2\cdot\mathbf{L})(\boldsymbol{\sigma}_1\cdot\mathbf{L})]. \tag{A2b}$$

For the basic functions for the Fourier transforms with Gaussian form factors, we refer to Refs. [3,36].

(a) Pseudoscalar-meson-exchange:

$$V_{\text{PS}}(r) = \frac{m}{4\pi}\left[f^P_{13}f^P_{24}\left(\frac{m}{m_{\pi^+}}\right)^2\left(\frac{1}{3}(\boldsymbol{\sigma}_1\cdot\boldsymbol{\sigma}_2)\,\phi^1_C + S_{12}\phi^0_T\right)\right], \tag{A3a}$$

$$V^{\text{n.l.}}_{\text{PS}}(r) = -\frac{m}{4\pi}\left[f^P_{13}f^P_{24}\left(\frac{m^2}{2m^2_{\pi^+}}\right)\left(\frac{1}{3}(\boldsymbol{\sigma}_1\cdot\boldsymbol{\sigma}_2)\,\phi^1_C + S_{12}\phi^0_T\right)\right]. \tag{A3b}$$

(b) Vector-meson exchange:

$$\begin{aligned}V_V(r) = \frac{m}{4\pi}\Bigg(&\left\{g^V_{13}g^V_{24}\left[\phi^0_C + \frac{m^2}{2M_YM_N}\phi^1_C\right] + \left[g^V_{13}f^V_{24}\frac{m^2}{4\mathcal{M}M_N} + f^V_{13}g^V_{24}\frac{m^2}{4\mathcal{M}M_Y}\right]\phi^1_C + f^V_{13}f^V_{24}\frac{m^4}{16\mathcal{M}^2M_YM_N}\phi^2_C\right\}\\
&+\frac{m^2}{6M_YM_N}\left\{\left[\left(g^V_{13}+f^V_{13}\frac{M_Y}{\mathcal{M}}\right)\left(g^V_{24}+f^V_{24}\frac{M_N}{\mathcal{M}}\right)\right]\phi^1_C + f^V_{13}f^V_{24}\frac{m^2}{8\mathcal{M}^2}\phi^2_C\right\}(\boldsymbol{\sigma}_1\cdot\boldsymbol{\sigma}_2)\\
&-\frac{m^2}{4M_YM_N}\left\{\left[\left(g^V_{13}+f^V_{13}\frac{M_Y}{\mathcal{M}}\right)\left(g^V_{24}+f^V_{24}\frac{M_N}{\mathcal{M}}\right)\right]\phi^0_T + f^V_{13}f^V_{24}\frac{m^2}{8\mathcal{M}^2}\phi^1_T\right\}S_{12}\\
&-\frac{m^2}{M_YM_N}\left\{\left[\frac{3}{2}g^V_{13}g^V_{24} + \left(g^V_{13}f^V_{24}+f^V_{13}g^V_{24}\right)\frac{\sqrt{M_YM_N}}{\mathcal{M}}\right]\phi^0_{SO} + \frac{3}{8}f^V_{13}f^V_{24}\frac{m^2}{\mathcal{M}^2}\phi^1_{SO}\right\}\mathbf{L}\cdot\mathbf{S}\\
&+\frac{m^4}{16M^2_YM^2_N}\left\{\left[g^V_{13}g^V_{24} + 4\left(g^V_{13}f^V_{24}+f^V_{13}g^V_{24}\right)\frac{\sqrt{M_YM_N}}{\mathcal{M}} + 8f^V_{13}f^V_{24}\frac{M_YM_N}{\mathcal{M}^2}\right]\right\}\cdot\\
&\times\frac{3}{(mr)^2}\phi^0_TQ_{12} - \frac{m^2}{M_YM_N}\left\{\left[\left(g^V_{13}g^V_{24} - f^V_{13}f^V_{24}\frac{m^2}{\mathcal{M}^2}\right)\frac{\left(M^2_N-M^2_Y\right)}{4M_YM_N} - \left(g^V_{13}f^V_{24} - f^V_{13}g^V_{24}\right)\frac{\sqrt{M_YM_N}}{\mathcal{M}}\right]\phi^0_{SO}\right\}\frac{1}{2}(\boldsymbol{\sigma}_1-\boldsymbol{\sigma}_2)\cdot\mathbf{L}\Bigg),\end{aligned} \tag{A4a}$$

$$\begin{aligned}V^{\text{n.l.}}_V(r) = \frac{m}{4\pi}\Bigg(&\frac{3}{2}g^V_{13}g^V_{24}\,\phi^0_C + \frac{m^2}{6M_YM_N}\left\{\left[\left(g^V_{13}+f^V_{13}\frac{M_Y}{\mathcal{M}}\right)\left(g^V_{24}+f^V_{24}\frac{M_N}{\mathcal{M}}\right)\right]\phi^1_C\right\}(\boldsymbol{\sigma}_1\cdot\boldsymbol{\sigma}_2)\\
&-\frac{m^2}{4M_YM_N}\left\{\left[\left(g^V_{13}+f^V_{13}\frac{M_Y}{\mathcal{M}}\right)\left(g^V_{24}+f^V_{24}\frac{M_N}{\mathcal{M}}\right)\right]\phi^0_T\right\}S_{12}\Bigg).\end{aligned} \tag{A4b}$$

Note: the spin-spin and tensor nonlocal terms are not included in ESC16.

[2]The relation with the nonlocal $\phi(r)$ function defined in Ref. [36], Eq. (35), and the $V^{\text{n.l.}}(r)$ is $\phi(r) = [2M_{\text{red}}/(2M_YM_N)]\,V^{\text{n.l.}}(r)$.

(c) Scalar-meson exchange:

$$V_S(r) = -\frac{m}{4\pi}\left(g^S_{13}g^S_{24}\left\{\left[\phi^0_C - \frac{m^2}{4M_YM_N}\phi^1_C\right] + \frac{m^2}{2M_YM_N}\phi^0_{SO}\,\mathbf{L}\cdot\mathbf{S} + \frac{m^4}{16M_Y^2M_N^2}\frac{3}{(mr)^2}\phi^0_T Q_{12} + \frac{m^2}{M_YM_N}\left[\frac{(M_N^2-M_Y^2)}{4M_YM_N}\right]\phi^0_{SO}\frac{1}{2}(\boldsymbol{\sigma}_1-\boldsymbol{\sigma}_2)\cdot\mathbf{L}\right\}\right), \tag{A5a}$$

$$V_S^{\text{n.l.}}(r) = \frac{m}{4\pi}\left[\frac{1}{2}g^S_{13}g^S_{24}\,\phi^0_C\right]. \tag{A5b}$$

(d) Axial-vector-meson exchange $J^{\text{PC}} = 1^{++}$:

$$V_A(r) = -\frac{m}{4\pi}\left(\left\{g^A_{13}g^A_{24}\left(\phi^0_C + \frac{2m^2}{3M_YM_N}\phi^1_C\right) + \frac{m^2}{6M_YM_N}\left(g^A_{13}f^A_{24}\frac{M_N}{\mathcal{M}} + f^A_{13}g^A_{24}\frac{M_Y}{\mathcal{M}}\right)\phi^1_C + f^A_{13}f^A_{24}\frac{m^4}{12M_YM_N\mathcal{M}^2}\phi^2_C\right\}(\boldsymbol{\sigma}_1\cdot\boldsymbol{\sigma}_2) - \frac{m^2}{4M_YM_N}\left\{\left[g^A_{13}g^A_{24} - 2\left(g^A_{13}f^A_{24}\frac{M_N}{\mathcal{M}} + f^A_{13}g^A_{24}\frac{M_Y}{\mathcal{M}}\right)\right]\phi^0_T - f^A_{13}f^A_{24}\frac{m^2}{\mathcal{M}^2}\phi^1_T\right\}S_{12} + \frac{m^2}{2M_YM_N}g^A_{13}g^A_{24}\left\{\phi^0_{SO}\,\mathbf{L}\cdot\mathbf{S} + \frac{m^2}{M_YM_N}\left[\frac{(M_N^2-M_Y^2)}{4M_YM_N}\right]\phi^0_{SO}\frac{1}{2}(\boldsymbol{\sigma}_1-\boldsymbol{\sigma}_2)\cdot\mathbf{L}\right\}\right), \tag{A6a}$$

$$V_A^{\text{n.l.}}(r) = -\frac{m}{4\pi}\left[\frac{3}{2}g^A_{13}g^A_{24}\,\phi^0_C(\boldsymbol{\sigma}_1\cdot\boldsymbol{\sigma}_2)\right]. \tag{A6b}$$

(e) Axial-vector-meson exchange $J^{\text{PC}} = 1^{+-}$:

$$V_B(r) = -\frac{m}{4\pi}\frac{(M_N+M_Y)^2}{m^2}\left\{f^B_{13}f^B_{24}\left[\frac{m^2}{12M_YM_N}\left(\phi^1_C + \frac{m^2}{4M_YM_N}\phi^2_C\right)(\boldsymbol{\sigma}_1\cdot\boldsymbol{\sigma}_2) + \frac{m^2}{4M_YM_N}\left(\phi^0_T + \frac{m^2}{4M_YM_N}\phi^1_T\right)S_{12}\right]\right\}, \tag{A7a}$$

$$V_B^{\text{n.l.}}(r) = -\frac{m}{4\pi}\frac{3(M_N+M_Y)^2}{8m^2}\left\{f^B_{13}f^B_{24}\left[\left(\frac{1}{3}\boldsymbol{\sigma}_1\cdot\boldsymbol{\sigma}_2\,\phi^1_C + S_{12}\,\phi^0_T\right)\right]\right\}. \tag{A7b}$$

(f) Pomeron exchange:

$$V_P(r) = \frac{m_P}{4\pi}\left[g^P_{13}g^P_{24}\frac{4}{\sqrt{\pi}}\frac{m_P^2}{\mathcal{M}^2}\left(\left\{1 + \frac{m_P^2}{2M_YM_N}\left(3-2m_P^2r^2\right) + \frac{m_P^2}{M_YM_N}\mathbf{L}\cdot\mathbf{S} + \left(\frac{m_P^2}{2M_YM_N}\right)^2 Q_{12} + \frac{m_P^2}{M_YM_N}\left[\frac{(M_N^2-M_Y^2)}{4M_YM_N}\right]\cdot\frac{1}{2}(\boldsymbol{\sigma}_1-\boldsymbol{\sigma}_2)\cdot\mathbf{L}\right\}e^{-m_P^2r^2}\right)\right], \tag{A8a}$$

$$V_D^{\text{n.l.}}(r) = -\frac{m}{4\pi}\left[\frac{1}{2}e^{-m_P^2r^2}\right]. \tag{A8b}$$

(g) Odderon-exchange:

$$V_{O,C}(r) = +\frac{g^O_{13}g^O_{24}}{4\pi}\frac{8}{\sqrt{\pi}}\frac{m_O^5}{\mathcal{M}^4}\left[\left(3-2m_O^2r^2\right) - \frac{m_O^2}{M_YM_N}\left(15-20m_O^2r^2+4m_O^4r^4\right)\right]\exp\left(-m_O^2r^2\right), \tag{A9a}$$

$$V_O^{\text{n.l.}}(r) = -\frac{g^O_{13}g^O_{24}}{4\pi}\frac{8}{\sqrt{\pi}}\frac{m_O^5}{\mathcal{M}^4}\frac{3}{4M_YM_N}\left\{\nabla^2\left[\left(3-2m_O^2r^2\right)\exp\left(-m_O^2r^2\right)\right] + \left[\left(3-2m_O^2r^2\right)\exp\left(-m_O^2r^2\right)\right]\nabla^2\right\}, \tag{A9b}$$

$$V_{O,\sigma}(r) = -\frac{g^O_{13}g^O_{24}}{4\pi}\frac{8}{3\sqrt{\pi}}\frac{m_O^5}{\mathcal{M}^4}\frac{m_O^2}{M_YM_N}\left[15-20m_O^2r^2+4m_O^4r^4\right]\exp\left(-m_O^2r^2\right)\left(1+\kappa^O_{13}\frac{M_Y}{\mathcal{M}}\right)\left(1+\kappa^O_{24}\frac{M_N}{\mathcal{M}}\right), \tag{A9c}$$

$$V_{O,T}(r) = -\frac{g^O_{13}g^O_{24}}{4\pi}\frac{8}{3\sqrt{\pi}}\frac{m_O^5}{\mathcal{M}^4}\frac{m_O^2}{M_YM_N}m_O^2r^2\left[7-2m_O^2r^2\right]\exp\left(-m_O^2r^2\right)\left(1+\kappa^O_{13}\frac{M_Y}{\mathcal{M}}\right)\left(1+\kappa^O_{24}\frac{M_N}{\mathcal{M}}\right), \tag{A9d}$$

$$V_{O,SO}(r) = -\frac{g^O_{13}g^O_{24}}{4\pi}\frac{8}{\sqrt{\pi}}\frac{m_O^5}{\mathcal{M}^4}\frac{m_O^2}{M_YM_N}\left[5-2m_O^2r^2\right]\exp\left(-m_O^2r^2\right)\cdot\left\{3+\left(\kappa^O_{13}+\kappa^O_{24}\right)\frac{\sqrt{M_YM_N}}{\mathcal{M}}\right\}, \tag{A9e}$$

$$V_{O,Q}(r) = +\frac{g^O_{13}g^O_{24}}{4\pi}\frac{2}{\sqrt{\pi}}\frac{m_O^5}{\mathcal{M}^4}\frac{m_O^4}{M_Y^2M_N^2}\left[7-2m_O^2r^2\right]\exp\left(-m_O^2r^2\right)\left\{1+4\left(\kappa^O_{13}+\kappa^O_{24}\right)\frac{\sqrt{M_YM_N}}{\mathcal{M}}+8\kappa_{13}\kappa_{24}\frac{M_YM_N}{\mathcal{M}^2}\right\}, \tag{A9f}$$

$$V_{\mathrm{O,ASO}}(r) = -\frac{g^O_{13}g^O_{24}}{4\pi}\frac{4}{\sqrt{\pi}}\frac{m_O^5}{\mathcal{M}^4}\frac{m_O^2}{M_Y M_N}\left[5-2m_O^2r^2\right]\exp\left(-m_O^2r^2\right)\left\{\frac{M_N^2-M_Y^2}{M_Y M_N}-4\left(\kappa^O_{24}-\kappa^O_{13}\right)\frac{\sqrt{M_Y M_N}}{\mathcal{M}}\right\}. \tag{A9g}$$

Here, $\kappa^O_{13} = g^O_{13}/f^O_{13}$ and $\kappa^O_{24} = g^O_{24}/f^O_{24}$.

One-boson-exchange interactions in configuration space II

Here we give the extra potentials due to the zeroes in the scalar and axial-A vector form factors:

(a) Scalar mesons:

$$\Delta V_S(r) = -\frac{m}{4\pi}\frac{m^2}{U^2}\left(g^S_{13}g^S_{24}\left\{\left[\phi^1_C-\frac{m^2}{4M_Y M_N}\phi^2_C\right]+\frac{m^2}{2M_Y M_N}\phi^1_{SO}\,\mathbf{L}\cdot\mathbf{S}+\frac{m^4}{16M_Y^2M_N^2}\phi^1_T\;Q_{12}\right.\right.$$
$$\left.\left.+\frac{m^2}{4M_Y M_N}\frac{M_N^2-M_Y^2}{M_Y M_N}\;\phi^{(1)}_{SO}\frac{1}{2}(\boldsymbol{\sigma}_1-\boldsymbol{\sigma}_2)\cdot\mathbf{L}\right\}\right). \tag{A10}$$

(b) Axial mesons: The extra contribution to the potentials coming from the zero in the axial-vector meson form factor are obtained from the expression $V_A(r)$ by making substitutions

$$\Delta V_A(1)(r) = V_A\left(\phi^0_C\to\phi^1_C,\phi^0_T\to\phi^1_T,\phi^0_{SO}\to\phi^1_{SO}\right)\frac{m^2}{U^2}. \tag{A11}$$

Note that we do not include the similar $\Delta V^{(2)}_A(r)$ since they involve $\mathbf{k}^4$ terms in momentum space. Then,

$$V^{(1)}_A(r) = -\frac{g^A_{13}g^A_{24}}{4\pi}\,m\left[\phi^1_C\,(\boldsymbol{\sigma}_1\cdot\boldsymbol{\sigma}_2)-\frac{1}{12M_Y M_N}\left(\nabla^2\phi^1_C+\phi^1_C\nabla^2\right)(\boldsymbol{\sigma}_1\cdot\boldsymbol{\sigma}_2)+\frac{3m^2}{4M_Y M_N}\;\phi^1_T\;S_{12}+\frac{m^2}{2M_Y M_N}\;\phi^1_{SO}\,\mathbf{L}\cdot\mathbf{S}\right.$$
$$\left.+\frac{m^2}{4M_Y M_N}\frac{M_N^2-M_Y^2}{M_Y M_N}\;\phi^{(1)}_{SO}\frac{1}{2}(\boldsymbol{\sigma}_1-\boldsymbol{\sigma}_2)\cdot\mathbf{L}\right]. \tag{A12}$$

APPENDIX B: NONLOCAL TENSOR CORRECTION

In this Appendix we repeat the treatment of the nonlocal correction correction to the tensor-potential similar to that for the central nonlocal potential

$$\Delta\widetilde{V}_T = \left(\mathbf{q}^2+\tfrac{1}{4}\mathbf{k}^2\right)\widetilde{v}_T\;S_{12}. \tag{B1}$$

This incorporation of this kind of potential in the solution of the Schrödinger equation is given in Ref. [46]; see Appendix B. For completeness we repeat here the treatment of this type of potential, which is exact when there is no nonlocal spin-orbit potential. For definiteness we consider the contribution to the π-exchange potential,

$$\widetilde{v}_T = \frac{f_P^2}{2MM'\,m_\pi^2}\left(\mathbf{q}^2+\frac{1}{4}\mathbf{k}^2\right)\Big/(\mathbf{k}^2+m^2). \tag{B2}$$

In configuration space this leads to the potential

$$V_T(r) = \frac{f_P^2}{4\pi}\frac{m}{4MM'}\left[\frac{1}{3}(\boldsymbol{\sigma}_1\cdot\boldsymbol{\sigma}_2)\left(\nabla^2\phi^1_C+\phi^1_C\nabla^2\right)+\left(\nabla^2\phi^0_T S_{12}+\phi^0_T S_{12}\nabla^2\right)\right]$$
$$\equiv -[(\nabla^2\phi(r)+\phi(r)\nabla^2)+(\nabla^2\chi(r)S_{12}+\chi(r)S_{12}\nabla^2)]. \tag{B3}$$

Here we put $\boldsymbol{\sigma}_1\cdot\boldsymbol{\sigma}_2 = 1$, because this potential contributes for spin-triplet states only. The radial Schrödinger equation reads

$$\{(1+2\phi)+2\chi\;S_12\}\,u''+(2\phi'+2\chi'\;S_{12})\,u'+\left[k^2_{\mathrm{cm}}-2M_{\mathrm{red}}V-\{(1+2\phi)+\chi\;S_{12}\}\frac{\mathbf{L}^2}{r^2}-\frac{\mathbf{L}^2}{r^2}\chi\;S_{12}+\phi''+\chi''\;S_{12}\right]u=0. \tag{B4}$$

Under the substitution $u = A^{-1/2}v$, where

$$A \equiv (1+2\phi)+2\chi\;S_{12}, \tag{B5}$$

over into the radial equation for $v(r)$,

$$v''(r)+\left[k^2_{\mathrm{cm}}-\frac{l(l+1)}{r^2}-2M_{\mathrm{red}}W\right]v(r)=0, \tag{B6}$$

with the (pseudo)potential

$$2M_{\rm red}W = 2M_{\rm red}A^{-1/2}V\,A^{-1/2} - A^{-2}(\phi' + \chi'\,S_{12})^2 - (A^{-1}-1)\,k_{\rm cm}^2 + \{A^{1/2}[L^2, A^{-1/2}] + A^{-1/2}[L^2, A^{1/2}]\}/(2r^2). \quad \text{(B7)}$$

In passing we note that A and S_{12} commute, and therefore

$$A^{-2}(\phi' + \chi'\,S_{12})^2 = [A^{-1/2}(\phi' + \chi'\,S_{12})A^{-1/2}]^2 = \tfrac{1}{4}[A^{-1/2}\,A'\,A^{-1/2}]^2.$$

Defining

$$X = (1 + 2\phi + 4\chi)^{1/2}\,, \quad Y = (1 + 2\phi - 8\chi)^{1/2}, \quad \text{(B8)}$$

the transformation A is given as

$$A^{1/2} = \tfrac{1}{3}(2X + Y) + \tfrac{1}{6}(X - Y)\,S_{12}, \quad A^{-1/2} = \left\{\tfrac{1}{3}(X + 2Y) + \tfrac{1}{6}(-X + Y)\,S_{12}\right\}/(XY). \quad \text{(B9)}$$

Using Eq. (B10) one readily derives

$$\{A^{1/2}[L^2, A^{-1/2}]_- + A^{-1/2}[L^2, A^{1/2}]_-\} = -2\frac{(X-Y)^2}{XY}\,\frac{\sqrt{J(J+1)}}{2J+1}\begin{pmatrix} 2\sqrt{J(J+1)} & -1 \\ -1 & -2\sqrt{J(J+1)}\end{pmatrix}. \quad \text{(B10)}$$

Writing $A^{-1} = \alpha + \beta\,S_{12}$ one finds

$$\alpha = +(1 + 2\phi - 4\chi)[(1 + 2\phi + 4\chi)(1 + 2\phi - 8\chi)]^{-1}, \quad \beta = -2\chi\,[(1 + 2\phi + 4\chi)(1 + 2\phi - 8\chi)]^{-1}, \quad \text{(B11)}$$

leading to

$$-(A^{-1} - 1) = \{[(2\phi - 8\chi)(1 + 2\phi + 4\chi) - 8\chi] + 2\chi\,S_{12}\}[(1 + 2\phi + 4\chi)(1 + 2\phi - 8\chi)]^{-1}. \quad \text{(B12)}$$

APPENDIX C: NEW VERSION QUARK-PAIR-CREATION MODEL [52]

In this Appendix we give a short description of the evaluation of the BBM coupling constants in the QPC model using the Fierz-transformation technique. For details we refer to Ref. [52]. Here, apart from the Fierz-transformation, the techniques used are those of Refs. [27,47,50]. In Fig. 7 the two kind of processes, direct (a) and exchange (b), are shown.

The derivation of the BBM couplings starts from the generalized $^3P_0$ (S) and $^3S_1$ (V) Pair-creation Hamiltonians

$$\mathcal{H}_I^{(S)} = -4\gamma_{q\bar{q}}^{(S)}\left(\sum_i \bar{q}_i q_i\right)\left(\sum_j \bar{q}_j q_j\right),$$

$$\mathcal{H}_I^{(V)} = -\gamma_{q\bar{q}}^{(V)}\left(\sum_i \bar{q}_{i,\alpha}(\boldsymbol{\lambda})^\alpha_{\ \beta}\gamma^\mu q_{i,\beta}\right)\otimes\left(\sum_j \bar{q}_{j,\gamma}(\boldsymbol{\lambda})^\gamma_{\ \delta}\gamma_\mu q_{j,\delta}\right), \quad \text{(C1)}$$

where $\gamma_{q\bar{q}}^{(V)}$ is a phenomenological constant, and the summations run as $i, j = u, d, s$. In this QPC model in the fundamental process there is a (confined) scalar or gluon propagator. This implies, assuming a constant propagator, an extra factor depending on a scalar or (massive) gluon exchange $(-i)^2(\mp i/m_G^2) \sim \pm i/\Lambda_{\rm QPC}^2$, meaning $\sim \pm i H_{\rm int}$.

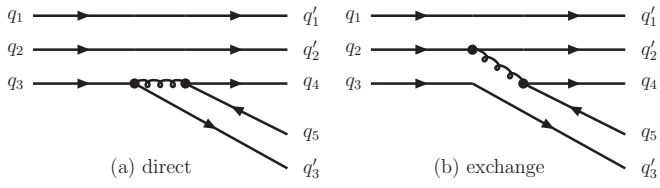

FIG. 7. $^3P_0$- and $^3S_1$-quark-pair creation (QPC).

Rearrangement is supposed to take place when a quark-antiquark pair is created by some mechanism in a baryon, where one quark from the baryon combines into a mesonic state with the antiquark from the pair. The quark from the pair recombines with the two remaining quarks of the baryon to make the baryon in the final state. This rearrangements into mesons of different kind can be understood from a Fierz-transformation applied to Eq. (C1). One has the identity [86]

$$\mathcal{H}_I^{(S)} = \gamma_{q\bar{q}}^{(S)}\sum_{i,j}\Big[+\ \bar{q}_i\,q_j \times \bar{q}_i\,q_j + \bar{q}_i\gamma_\mu q_j \times \bar{q}_j\gamma^\mu q_i - \frac{1}{2}\,\bar{q}_i\sigma_{\mu\nu}q_j \times \bar{q}_j\sigma^{\mu\nu}q_i - \bar{q}_i\gamma_\mu\gamma_5 q_j \times \bar{q}_j\gamma^\mu\gamma^5 q_i + \bar{q}_i\gamma_5 q_j \times \bar{q}_j\gamma^5 q_i\Big],$$

$$\mathcal{H}_I^{(V)} = +\gamma_{q\bar{q}}^{(V)}\sum_{i,j}\Big[+\ \bar{q}_i\,q_j \times \bar{q}_i\,q_j - \frac{1}{2}\,\bar{q}_i\gamma_\mu q_j \times \bar{q}_j\gamma^\mu q_i - \frac{1}{2}\,\bar{q}_i\gamma_\mu\gamma_5 q_j \times \bar{q}_j\gamma^\mu\gamma^5 q_i - \bar{q}_i\gamma_5 q_j \times \bar{q}_j\gamma^5 q_i\Big]. \quad \text{(C2)}$$

Here, we considered only the flavor-spin Fierzing.[3] The appropriate Fierzing of the color structure is different for diagram (a) and diagram (b) in Fig. 7: (i) For diagram (a) we use

[3]It should be noted that the terms for the couplings of the B-axial $J^{\rm PC} = 1^{+-}$ and tensor $J^{\rm PC} = 2^{++}$ mesons are missing on the right-hand side of Eq. (C2). The same is true for the $^3P_0$-interaction Eq. (C1).

the identity [86]

$$(\boldsymbol{\lambda})^{\gamma}_{\delta}\cdot(\boldsymbol{\lambda})_{\alpha}^{\beta}=\tfrac{16}{9}\delta_{\alpha}^{\gamma}\delta_{\delta}^{\beta}-\tfrac{1}{3}(\boldsymbol{\lambda})^{\gamma}_{\alpha}\cdot(\boldsymbol{\lambda})^{\beta}_{\delta}. \tag{C3}$$

Since the mesons are colorless, the second term in Eq. (C3) may be neglected, and color gives the simple factor 16/9.

(ii) In diagram (b) there is in fact a sum over q_1 and q_2. Because the baryons are colorless, we have

$$(\boldsymbol{\lambda}_1)_{\alpha}^{\beta}+(\boldsymbol{\lambda}_2)_{\alpha}^{\beta}=-(\boldsymbol{\lambda}_3)_{\alpha}^{\beta}. \tag{C4}$$

Therefore, for this diagram we have, using Eq. (C3), the identity

$$(\boldsymbol{\lambda}_5)^{\gamma}_{\delta}\cdot\sum_{i=1,2}(\boldsymbol{\lambda}_i)_{\alpha}^{\beta}=-\frac{16}{9}\delta_{\alpha}^{\gamma}\delta_{\delta}^{\beta}+\frac{1}{3}(\boldsymbol{\lambda}_5)^{\gamma}_{\alpha}\cdot(\boldsymbol{\lambda}_3)^{\beta}_{\delta} \tag{C5}$$

Again, for colorless mesons the second term in Eq. (C5) may be neglected, and color gives the simple factor $-16/9$.

We find that the direct (a) and exchange (b) diagram give different color factors. Such a difference does not occur in the $^3P_0$ model. Now, it appears that the momentum overlap for type (b) is usually much smaller than for type (a); see Ref. [52] for details. This can be traced back to our use of a constant propagator for the (confined) gluon. Therefore, in the following we neglect processes described in diagram (b). Then, the difference between the $^3P_0$ and $^3S_1$ model is, apart from an overall constant, exclusively given by the different coefficients in the flavor-spin Fierz-identities Eq. (C2).

In the $^3S_1$ model for the interaction Hamiltonian for the pair-creation one uses the one-gluon-exchange (OGE) model [87,88]; see Fig. 7. Considering one-gluon exchange, see Fig. 7, one derives the effective vertex [87,88] by using a (confined) constant $P_g(ji)$ gluon propagator between quark line i and line j: $P_g(ji)\sim\delta_{ji}/m_g^2$, where the (effective) gluon mass is taken to be $m_g\approx(0.8fm^{-1})\approx 250\,\mathrm{MeV}$ [88]. We notice that the color factor for the coupling of colorless mesons to colorless baryons is always the same, and we can include this into an effective coupling γ_S, i.e.,

$$\frac{\pi\alpha_s(\boldsymbol{\lambda}_i\cdot\boldsymbol{\lambda}_j)}{m_G^2}\Rightarrow\gamma_{q\bar{q}}^{(V)}. \tag{C6}$$

Here we use for the gluon a constant (confined) propagator $P_g=1/m_G^2$. As is clear from (C1) $\gamma_{q\bar{q}}$ has the dimension $[\mathrm{MeV}]^{-2}$. Also, we notice that $m_G\approx\Lambda_{\mathrm{QPC}}$, therefore $\gamma_{q\bar{q}}\longrightarrow\gamma_{q\bar{q}}/\Lambda^2_{\mathrm{QPC}}$. From the momentum conservation rules one now gets different dependencies between the momenta as compared to the version of the $^3P_0$ model in Refs. [27,50]. Hence, we have different momentum overlap integrals.

From the results for the couplings of the mesons in the $^3P_0$ model those for the $^3S_1$-model meson-couplings can be read off by comparing the coefficients in the Fierz-identities Eqs. (C2) and (C1) for the corresponding operators. Here, we assume that the effect of color in the $^3P_0$ and $^3S_1$ model can be absorbed into $\gamma_{q\bar{q}}^{(S,V)}$, see below. For example, the prediction for the scalar-meson couplings will have the ratio $g_\epsilon(^3S_1)=[\gamma_{q\bar{q}}^{(V)}/\gamma_{q\bar{q}}^{(S)}]g_\epsilon(^3P_0)$. Apart from an overall constant, the couplings for the $^3S_1$ model can be read off from those of the $^3P_0$ model.

1. Meson states, meson and baryon wave functions

We list the $\langle B,M|H_{\mathrm{int}}|A\rangle$ matrix elements for the different type of mesons. Restriction on the quark-level to process (a) in Fig. 7, using the Fierzed form of the interaction Hamiltonians in Eq. (C1). So, below we will give the results for the $^3P_0$ model. Following Ref. [48], we write the meson creation operators as

$$J^{\mathrm{PC}}=0^{-+}:\ d^{\dagger}_{M,P}(\mathbf{k})=i\sum_{r,s=\pm}\int d^3k_1d^3k_2\,\delta(\mathbf{k}-\mathbf{k}_1-\mathbf{k}_2)\widetilde{\psi}_M^{(L=0)}(\mathbf{k}_1,\mathbf{k}_2)\,\varphi^{(0)}(r,s)\,b^{\dagger}(\mathbf{k}_1,r)\,d^{\dagger}(\mathbf{k}_2,s), \tag{C7}$$

$$J^{\mathrm{PC}}=1^{--}:\ d^{\dagger}_{M,V}(\mathbf{k},m)=\sum_{r,s=\pm}\int d^3k_1d^3k_2\,\delta(\mathbf{k}-\mathbf{k}_1-\mathbf{k}_2)\widetilde{\psi}_M^{(L=0)}(\mathbf{k}_1,\mathbf{k}_2)\,\varphi^{(1)}_m(r,s)\,b^{\dagger}(\mathbf{k}_1,r)\,d^{\dagger}(\mathbf{k}_2,s), \tag{C8}$$

$$J^{\mathrm{PC}}=0^{++}:\ d^{\dagger}_{M,S}(\mathbf{k},m)=\sum_{r,s=\pm}\int d^3k_1d^3k_2\,\delta(\mathbf{k}-\mathbf{k}_1-\mathbf{k}_2)\,(-)^m\widetilde{\psi}_{M,m}^{(L=1)}(\mathbf{k}_1,\mathbf{k}_2)\,\varphi^{(1)}_{-m}(r,s)\,b^{\dagger}(\mathbf{k}_1,r)\,d^{\dagger}(\mathbf{k}_2,s), \tag{C9}$$

$$J^{\mathrm{PC}}=1^{++}:\ d^{\dagger}_{M,A}(\mathbf{k},m)=\sum_{r,s=\pm}\int d^3k_1d^3k_2\,\delta(\mathbf{k}-\mathbf{k}_1-\mathbf{k}_2)\,C(1,1,1;m_L,m_\sigma,m)\widetilde{\psi}_{M,m_L}^{(L=1)}(\mathbf{k}_1,\mathbf{k}_2)\,\varphi^{(1)}_{m_\sigma}(r,s)\,b^{\dagger}(\mathbf{k}_1,r)\,d^{\dagger}(\mathbf{k}_2,s), \tag{C10}$$

$$J^{\mathrm{PC}}=1^{+-}:\ d^{\dagger}_{M,B}(\mathbf{k},m)=\sum_{r,s=\pm}\int d^3k_1d^3k_2\,\delta(\mathbf{k}-\mathbf{k}_1-\mathbf{k}_2)\widetilde{\psi}_{M,m}^{(L=1)}(\mathbf{k}_1,\mathbf{k}_2)\,\varphi^{(0)}(r,s)\,b^{\dagger}(\mathbf{k}_1,r)\,d^{\dagger}(\mathbf{k}_2,s), \tag{C11}$$

$$J^{\mathrm{PC}}=2^{++}:\ d^{\dagger}_{M,T}(\mathbf{k},m)=\sum_{r,s=\pm}\int d^3k_1d^3k_2\,\delta(\mathbf{k}-\mathbf{k}_1-\mathbf{k}_2)\,C(1,1,2;m_L,m_\sigma,m)\widetilde{\psi}_{M,m_L}^{(L=1)}(\mathbf{k}_1,\mathbf{k}_2)\,\varphi^{(1)}_{m_\sigma}(r,s)\,b^{\dagger}(\mathbf{k}_1,r)\,d^{\dagger}(\mathbf{k}_2,s), \tag{C12}$$

for, respectively, the pseudoscalar, vector, scalar, and axial-vector mesons of the first (A_1, etc.) and second kind (B_1, etc.), and tensor mesons. These representations are the equal-time Bethe-Salpeter wave functions [89]:

$$f_{\mathbf{k},\alpha}(x,y)\equiv\langle 0|T[q_i(x)q_j(y)]|M(\mathbf{k},\alpha\rangle\overset{x^0=y^0}{\longrightarrow}(0|q_i(\mathbf{x})q_j(\mathbf{y})|M(\mathbf{k},\alpha),$$

using the definition $\theta[0] = 1/2$. Here, a factor i is included in the definition of the $d^{\dagger}_{M,P}(\mathbf{k})$ operator. This to have under time-reversal $\mathcal{T}|\pi_0(\mathbf{k})\rangle = |\pi_0(-\mathbf{k})\rangle$. The reason is that under time-reversal the spin-components change sign, which implies for the spin-singlet $\varphi^{(0)}(-r,-s) = -\varphi^{(0)}(r,s)$, etc.

The baryon and meson harmonic oscillator wave functions are

$$\widetilde{\psi}_N(\mathbf{k}_1,\mathbf{k}_2,\mathbf{k}_3) = \left(\frac{\sqrt{3}R_A^2}{\pi}\right)^{3/2} \exp\left[-\frac{R_A^2}{6}\sum_{i<j}(\mathbf{k}_i-\mathbf{k}_j)^2\right],$$

$$\widetilde{\psi}^{(L=0)}_M(\mathbf{k}_1,\mathbf{k}_2) = \left(\frac{R_M^2}{\pi}\right)^{3/4} \exp\left[-\frac{R_M^2}{8}(\mathbf{k}_1-\mathbf{k}_2)^2\right],$$

$$\widetilde{\psi}^{(L=1)}_{M,m}(\mathbf{k}_1,\mathbf{k}_2) = \frac{R_M}{\sqrt{2}}\left(\frac{R_M^2}{\pi}\right)^{3/4} [-\boldsymbol{\epsilon}_m(\mathbf{k}_1-\mathbf{k}_2)] \times \exp\left[-\frac{R_M^2}{8}(\mathbf{k}_1-\mathbf{k}_2)^2\right].$$

Here we used the spherical unit vectors $\boldsymbol{\epsilon}_{\pm 1} = \mp\frac{1}{\sqrt{2}}(\mathbf{e}_1 \pm i\mathbf{e}_2)$, $\boldsymbol{\epsilon}_0 = \mathbf{e}_3$.

2. Coupling-constant formulas

The matrix elements $\langle B_f(\mathbf{p}')\, M(\mathbf{k})|\mathcal{H}_I^{(S),(V)}|B_i(\mathbf{p})\rangle$ involve the momentum space overlap integrals, which can be performed in a straightforward manner [52]. The summary of the derived formulas in Ref. [52], in the case of the $^3P_0$ model, for the divers ($I = 1$) couplings is

$$g_P = +\pi^{-3/4}\,\gamma_{q\bar{q}}\,\frac{(m_P R_P)^{1/2}}{(\Lambda_{\rm QPC}R_P)^2}(6\sqrt{2}),$$

$$g_V = +\pi^{-3/4}\,\gamma_{q\bar{q}}\,\frac{(m_V R_V)^{1/2}}{(\Lambda_{\rm QPC}R_V)^2}(3/\sqrt{2}),$$

$$g_S = +\pi^{-3/4}\,\gamma_{q\bar{q}}\,\frac{(m_S R_S)^{-1/2}}{(\Lambda_{\rm QPC}R_S)^2}\frac{9m_S}{M_B},$$

$$g_A = -\pi^{-3/4}\,\gamma_{q\bar{q}}\,\frac{(m_A R_A)^{-1/2}}{(\Lambda_{\rm QPC}R_A)^2}\frac{6m_A}{M_B},$$

with $\Lambda_{\rm QPC} \approx 600\,\text{MeV}$ and $R_M \approx 0.66$.

[1] Th. A. Rijken, in *Proceedings of the 14th European Conference on Few-Body Problems in Physics, Amsterdam 1993*, edited by B. Bakker and R. van Dantzig, Few-Body Systems Suppl 7, 1 (Springer, Berlin, 1994).
[2] M. M. Nagels, T. A. Rijken, and J. J. deSwart, Phys. Rev. D **15**, 2547 (1977).
[3] P. M. M. Maessen, Th. A. Rijken, and J. J. de Swart, Phys. Rev. C **40**, 2226 (1989).
[4] J. J. de Swart, Rev. Mod. Phys. **35**, 916 (1963). Here, the ratio $\alpha \equiv F/(F+D)$ is defined in Eq. (17.7).
[5] Th. A. Rijken, Phys. Rev. C **73**, 044007 (2006).
[6] Th. A. Rijken and Y. Yamamoto, Phys. Rev. C **73**, 044008 (2006).
[7] Th. A. Rijken and Y. Yamamoto, Extended-soft-core baryon-baryon model III. $S = -2$ hyperon-hyperon/nucleon interaction, arXiv:nucl-th/0608074.
[8] Th. A. Rijken, M. M. Nagels, and Y. Yamamoto, Nucl. Phys. A **835**, 160 (2010).
[9] Th. A. Rijken, M. M. Nagels, and Y. Yamamoto, Prog. Theor. Phys. Suppl. No. **185**, 14 (2010).
[10] Th. A. Rijken, V. G. J. Stoks, and Y. Yamamoto, Phys. Rev. C **59**, 21 (1999).
[11] V. G. J. Stoks, R. A. M. Klomp, M. C. M. Rentmeester, and J. J. de Swart, Phys. Rev. C **48**, 792 (1993).
[12] R. A. M. Klomp, private communication (unpublished).
[13] O. Hashimoto and H. Tamura, Prog. Part. Nucl. Phys. **57**, 564 (2006).
[14] H. Takahashi *et al.*, Phys. Rev. Lett. **87**, 212502 (2001).
[15] M. M. Nagels, Th. A. Rijken, and Y. Yamamoto, Phys. Rev. C **99**, 044003 (2019).
[16] M. M. Nagels, Th. A. Rijken, and Y. Yamamoto, *Extended-soft-core Baryon-baryon Model ESC16. III. Hyperon-hyperon Interactions* (unpublished).
[17] A. Manohar and H. Georgi, Nucl. Phys. B **234**, 189 (1984).
[18] G. A. Miller, Phys. Rev. C **39**, 1563 (1989).
[19] P. V. Landshoff and O. Nachtmann, Z. f. Physik C **35**, 405 (1987).
[20] F. J. Ynduráin, *Quantum Chromodynamics* (Springer, Berlin, 1980); see chapter IV for a description and references original literature.
[21] J. Gasser and H. Leutwyler, Nucl. Phys. B **94**, 269 (1975).
[22] S. Gasiorowicz and J. L. Rossner, Am. J. Phys. **49**, 954 (1981). Here, one uses the constituent quark masses: $m_u = m_d = 310\,\text{MeV}$ and $m_s = 483\,\text{MeV}$.
[23] B. Povh *et al.*, *Particles and Nuclei* (Springer, Berlin, 1995).
[24] H. D. Politzer, Nucl. Phys. B **117**, 397 (1976).
[25] M. Lavelle and D. McMullan, Phys. Rep. **279**, 1 (1997). In this reference an extensive discussion of the dressing-problem can be found.
[26] L. Micu, Nucl. Phys. B **10**, 521 (1969); R. Carlitz and M. Kislinger, Phys. Rev. D **2**, 336 (1970).
[27] A. Le Yaouanc, L. Oliver, O. Péne, and J.-C. Raynal, Phys. Rev. D **8**, 2223 (1973); **11**, 1272 (1975).
[28] This pair-creation mechanism has been shown to be dominant in Lattice QCD. See: N. Isgur and J. Paton, Phys. Rev. D **31**, 2910 (1985).
[29] J. Schwinger, Phys. Rev. Lett. **18**, 923 (1967); Phys. Rev. **167**, 1432 (1968); *Particles and Sources* (Gordon and Breach, Science Publishers, Inc., New York, 1969).
[30] S. Weinberg, Phys. Phys. **166**, 1568 (1968); **177**, 2604 (1969).
[31] V. De Alfaro, S. Fubini, G. Furlan, and C. Rosetti, *Currents in Hadron Physics*, Ch. 5 (North-Holland Publishing Company, Amsterdam, 1973).
[32] C. Patrignani *et al.* (Particle Data Group), Chin. Phys. C **40**, 100001 (2016).
[33] M. Gell-Mann, Phys. Rev. **125**, 1067 (1962); S. Okubo, Prog. Theor. Phys. **27**, 949 (1962); **28**, 24 (1962).
[34] V. G. J. Stoks and Th. A. Rijken, Nucl. Phys. A **613**, 311 (1997).

[35] M. Ablikim *et al.*, Phys. Lett. B **645**, 19 (2007). In this analysis of the $J/\psi \to \omega\pi^+\pi^-$ data the ε pole is at $E(\varepsilon) = (552 - i232)$ MeV, which corresponds to $m_\varepsilon = 620$ MeV, $\Gamma_\varepsilon = 464$ MeV.

[36] M. M. Nagels, Th. A. Rijken, and J. J. de Swart, Phys. Rev. D **17**, 768 (1978).

[37] Th. A. Rijken, Ann. Phys. (NY) **208**, 253 (1991).

[38] Th. A. Rijken and V. G. J. Stoks, Phys. Rev. C **54**, 2851 (1996).

[39] Th. A. Rijken and V. G. J. Stoks, Phys. Rev. C **54**, 2869 (1996).

[40] F. E. Low, Phys. Rev. D **12**, 163 (1975).

[41] S. Nussinov, Phys. Rev. Lett. **34**, 1286 (1975).

[42] J. J. de Swart, T. A. Rijken, P. M. Maessen, and R. G. E. Timmermans, Nuov. Cim. A **102**, 203 (1989).

[43] S. Otsuki, R. Tamagaki, and W. Wada, Progr. Theor. Phys. **32**, 220 (1964); S. Otsuki, R. Tamagaki, and M. Yasuno, Prog. Theor. Phys. Suppl. **E65**, 578 (1965).

[44] M. Oka, K. Shimizu, and K. Yazaki, Progr. Theor. Phys. Suppl. **137**, 1 (2000).

[45] Y. Fujiwara, Y. Suzuki, and C. Nakamoto, Prog. Part. Nucl. Phys. **58**, 439 (2007).

[46] M. M. Nagels, T. A. Rijken, and J. J. de Swart, N-N Potentials from Regge-Pole Theory, in *Few body Systems and Nuclear Forces I, Proceedings Graz 1978*, edited by H. Zingl, M. Haftel, and H. Zankel (Springer-Verlag, Berlin/Heidelberg/New York, 1978).

[47] A. Le Yaouanc, L. Oliver, O. Péne, and J.-C. Raynal, Phys. Rev. D **12**, 2137 (1975); **18**, 1591 (1978).

[48] R. van Royen and V. F. Weisskopf, Nuovo Cimento A **50**, 617 (1967).

[49] E. Leader and E. Predazzi, *An Introduction to Gauge Theories and Modern Particle Physics*, Cambridge Monographs on Particle Physics, Nuclear Physics and Cosmology, edited by T. Ericson and P. V. Landshoff (Cambridge University Press, Cambridge, 1996), Vol. I, Chap. 12.

[50] M. Chaichian and R. Kögerler, Ann. Phys. **124**, 61 (1980).

[51] K. Hagiwara *et al.* (Particle Data Group), Phys. Rev. D **66**, 010001 (2002).

[52] Th. A. Rijken, *Baryon-baryon Couplings in the* $^3P_0$ *and* $^3S_1$ *QPC-models*, Notes University of Nijmegen, Nijmegen, The Netherlands, *NN-online, THEF 12.01*.

[53] Th. A. Rijken, *Nucleon-Nucleon Interactions*, talk at KITPC workshop on Present Status Nuclear Interaction Theory, Beijing, August (2014).

[54] Y. Yamamoto, T. Motoba, and Th. A. Rijken, Prog. Theor. Phys. Suppl. **185**, 72 (2010).

[55] R. A. Bryan and A. Gersten, Phys. Rev. D **6**, 341 (1972).

[56] D. V. Bugg and R. A. Bryan, Nucl. Phys. A **540**, 449 (1992).

[57] V. G. J. Stoks, R. A. M. Klomp, C. P. F. Terheggen, and J. J. de Swart, Phys. Rev. C **49**, 2950 (1994).

[58] M. M. Nagels, Th. A. Rijken, J. J. deSwart, G. C. Oades, J. L. Petersen, A. C. Irving, C. Jarlskog, W. Pfeil, H. Pilkuhn, and H. P. Jacob, Nucl. Phys. B **147**, 189 (1979).

[59] D. E. Gonzales Trotter *et al.*, Phys. Rev. Lett. **83**, 3788 (1999).

[60] V. Huhn, L. Watzold, C. Weber, A. Siepe, W. von Witsch, H. Witala, and W. Glöckle, Phys. Rev. Lett. **85**, 1190 (2000).

[61] G. A. Miller, B. M. K. Nefkens, and I. Šlaus, Phys. Rep. **194**, 1 (1990).

[62] E. Epelbaum, H.-W. Hammer, and U.-G. Meissner, Rev. Mod. Phys. **81**, 1773 (2009).

[63] A. Andronic, P. Braun-Munzinger, and J. Stachel, Phys. Lett. B **673**, 142 (2009).

[64] R. Kokoski and N. Isgur, Phys. Rev. D **35**, 907 (1987).

[65] S. Kumano and V. R. Pandharipande, Phys. Rev. D **38**, 146 (1988).

[66] R. Navarro Pérez, J. E. Amaro, and E. Ruiz Arriola, Phys. Rev. C **88**, 024002 (2013).

[67] B. von Przewoski *et al.*, Phys. Rev. C **58**, 1897 (1998).

[68] C. E. Allgower, J. Ball, L. S. Barabash, P. Y. Beauvais, M. E. Beddo, N. Borisov, A. Boutefnouchet, J. Bystricky, P. A. Chamouard, M. Combet, P. Demierre, J. M. Fontaine, V. Ghazikhanian, D. P. Grosnick, R. Hess, Z. Janout, Z. F. Janout, V. A. Kalinnikov, T. E. Kasprzyk, Y. M. Kazarinov, B. A. Khachaturov, R. Kunne, F. Lehar, A. deLesquen, D. Lopiano, M. deMali, V. N. Matafonov, I. L. Pisarev, A. A. Popov, A. N. Prokofiev, D. Rapin, J. L. Sans, H. M. Spinka, Y. A. Usov, V. V. Vikhrov, B. Vuaridel, C. A. Whitten, and A. A. Zhdanov, Phys. Rev. C **62**, 064001 (2000).

[69] I. E. Lagaris and V. R. Pandharipande, Nucl. Phys. A **359**, 349 (1981).

[70] H.-J. Schulze and Th. A. Rijken, Phys. Rev. C **84**, 035801 (2011).

[71] M. Baldo, G. F. Burgio, and H.-J. Schulze, Phys. Rev. C **61**, 055801 (2000).

[72] I. Vidana, A. Polls, A. Ramos, L. Engvik, and M. Hjorth-Jensen, Phys. Rev. C **62**, 035801 (2000).

[73] S. Nishizaki, Y. Yamamoto, and T. Takatsuka, Prog. Theor. Phys. **105**, 607 (2001); **108**, 703 (2002).

[74] A. B. Kaidalov and K. A. Ter-Martirosian, Nucl. Phys. B **75**, 471 (1974).

[75] J. B. Bronzan and R. L. Sugar, Phys. Rev. D **16**, 466 (1977).

[76] Th. A. Rijken, *Multiple-Pomeron Coupling and the Universal Repulsion in Nuclear/Hyperonic Matter. I. Triple-Pomeron Vertices*, notes Nijmegen 2005 (unpublished).

[77] Th. A. Rijken, *Multi-Pomeron Exchange and the Universal Repulsion in Nuclear/Hyperonic Matter*, NN-online, THEF 08.01.

[78] Y. Yamamoto, T. Furumoto, N. Yasutake, and Th. A. Rijken, Phys. Rev. C **88**, 022801(R) (2013).

[79] Y. Yamamoto, T. Furumoto, N. Yasutake, and Th. A. Rijken, Phys. Rev. C **90**, 045805 (2014).

[80] Y. Yamamoto, T. Furumoto, N. Yasutake, and Th. A. Rijken, Eur. Phys. J. A **52**, 19 (2016).

[81] Y. Yamamoto, H. Togashi, T. Tamagawa, T. Furumoto, N. Yasutake, and Th. A. Rijken, Phys. Rev. C **96**, 065804 (2017).

[82] P. B. Demorest, T. Pennucci, S. M. Ransom, M. S. E. Roberts, and J. W. Hessels, Nature(London) **467**, 1081 (2010).

[83] J. Antoniadis *et al.*, Science **340**, 1233232 (2013).

[84] R. R. Scheerbaum, Nucl. Phys. A **257**, 77 (1976).

[85] E. Hiyama, M. Kamimura, T. Motoba, T. Yamada, and Y. Yamamoto, Phys. Rev. Lett. **85**, 270 (2000).

[86] L. B. Okun, *Leptons and Quarks*, Chap. 29, (North-Holland Publishing Company, Amsterdam, 1984).

[87] A. De Rújula, H. Georgi, and S. L. Glashow, Phys. Rev. D **12**, 147 (1975).

[88] E. M. Henley and Z.-Y. Zhang, Nucl. Phys. A **472**, 759 (1987).

[89] M. Gell-Mann and F. Low, Phys. Rev. **84**, 350 (1951).